LKB1 kinase-dependent and -independent defects disrupt polarity and adhesion signaling to drive collagen remodeling during invasion

Jessica Konen[a,b,†], Scott Wilkinson[a,b,†], Byoungkoo Lee[c], Haian Fu[a,d], Wei Zhou[a], Yi Jiang[c], and Adam I. Marcus[a,*]

[a]Department of Hematology and Medical Oncology, Winship Cancer Institute of Emory University, Atlanta, GA 30322;
[b]Graduate Program in Cancer Biology and [d]Department of Pharmacology, Emory University, Atlanta, GA 30322;
[c]Department of Mathematics and Statistics, Georgia State University, Atlanta, GA 30302

ABSTRACT **LKB1 is a serine/threonine kinase and a commonly mutated gene in lung adenocarcinoma. The majority of LKB1 mutations are truncations that disrupt its kinase activity and remove its C-terminal domain (CTD). Because LKB1 inactivation drives cancer metastasis in mice and leads to aberrant cell invasion in vitro, we sought to determine how compromised LKB1 function affects lung cancer cell polarity and invasion. Using three-dimensional models, we show that LKB1 kinase activity is essential for focal adhesion kinase–mediated cell adhesion and subsequent collagen remodeling but not cell polarity. Instead, cell polarity is overseen by the kinase-independent function of its CTD and more specifically its farnesylation. This occurs through a mesenchymal-amoeboid morphological switch that signals through the Rho-GTPase RhoA. These data suggest that a combination of kinase-dependent and -independent defects by LKB1 inactivation creates a uniquely invasive cell with aberrant polarity and adhesion signaling that drives invasion into the microenvironment.**

Monitoring Editor
Mark H. Ginsberg
University of California, San Diego

Received: Aug 10, 2015
Revised: Feb 5, 2016
Accepted: Feb 5, 2016

INTRODUCTION

Liver kinase B1 (LKB1; also known as STK11) is a serine/threonine kinase that was identified as a tumor suppressor in the inherited autosomal-dominant disorder Peutz–Jeghers syndrome (PJS). PJS patients have LKB1 loss of heterozygosity, resulting in gastrointestinal polyposis and a greater likelihood of developing sporadic tumors in the breast, gastrointestinal tract, and pancreas (Yoon *et al.*, 2000). Somatic inactivation of LKB1 is observed in several cancer types, including melanoma, lung, and cervical cancers (Guldberg *et al.*, 1999; Sanchez-Cespedes *et al.*, 2002; Matsumoto *et al.*, 2007; Wingo *et al.*, 2009). In lung adenocarcinoma, *LKB1* is the third most commonly mutated gene behind *KRAS* and *P53* (Ding *et al.*, 2008; Cancer Genome Atlas Research Network, 2014), although how *LKB1* mutations drive lung adenocarcinoma progression remains an area of intense interest.

LKB1 missense and truncating mutations in lung adenocarcinoma primarily occur within its central kinase domain (Cancer Genome Atlas Research Network, 2014). LKB1 kinase activity was first linked to the canonical 5′-AMP–activated protein kinase (AMPK) energy stress response pathway, where it serves as the upstream kinase of AMPK (Hawley *et al.*, 2003; Shaw *et al.*, 2004). LKB1 also phosphorylates and activates 14 members of the AMPK family (Lizcano *et al.*, 2004; Jaleel *et al.*, 2005; Hardie and Alessi, 2013), including the microtubule affinity–regulating kinases (MARK1–4; Spicer *et al.*, 2003; Brajenovic *et al.*, 2004; Lizcano *et al.*, 2004), and NUAK1/2 (Zagórska *et al.*, 2010; Vallenius *et al.*, 2011) to control myosin contractility, SIK1 to oversee anoikis (Cheng *et al.*, 2009), and the brain-specific kinases to promote axon differentiation (Barnes *et al.*, 2007; Kishi *et al.*, 2005).

The LKB1 kinase domain is flanked by a short N-terminal domain and a longer C-terminal domain (CTD) containing a membrane-targeting farnesylation motif (Hezel and Bardeesy, 2008; Houde *et al.*, 2014). Predictably, LKB1-truncating mutations within its kinase domain disrupt kinase function and result in a truncated protein lacking the CTD or a fully degraded transcript with complete protein loss.

This article was published online ahead of print in MBoC in Press (http://www.molbiolcell.org/cgi/doi/10.1091/mbc.E15-08-0569) on February 10, 2016.

†These authors contributed equally to this work.

*Address correspondence to: Adam Marcus (aimarcu@emory.edu).

Abbreviations used: AMPK, AMP-activated protein kinase; CTD, C-terminal domain; FAK, focal adhesion kinase; MARK, microtubule affinity-regulating kinase.

This observation raises the intriguing question of how loss of kinase activity, compared with loss of the CTD, affects LKB1 function and cancer progression. One possible answer could be linked to its role in cell polarity; LKB1 serves as a master regulator of cell polarity across multiple species (Marcus and Zhou, 2010; Nakano and Takashima, 2012). In *Caenorhabditis elegans*, the LKB1 orthologue PAR-4 is critical for establishing and maintaining an anterior-posterior (AP) axis during cell division (Watts *et al.*, 2000). In addition, in *Drosophila*, LKB1 is essential for establishing the AP axis during oogenesis and promoting an apical-basal polarity in eye and follicular cells (Martin and St Johnston, 2003; Amin *et al.*, 2009). In single human intestinal epithelial cells, LKB1 reexpression leads to a fully polarized cell, even in the absence of cell–cell contacts (Baas *et al.*, 2004). LKB1 loss in epithelial cells also disrupts apical-basal polarity and basement membrane integrity while promoting an epithelial-to-mesenchymal transition (Roy *et al.*, 2010; Partanen *et al.*, 2012). The role of LKB1 in regulating cell polarity and motility has linked LKB1 to the Rho family of small GTPases (Etienne-Manneville, 2004; Asada *et al.*, 2007). On activation of cell motility in lung cancer cell lines, LKB1 rapidly translocates to the cellular leading edge, where it binds to actin and associates with the small Rho-GTPase cdc42 (Zhang *et al.*, 2008). In addition, in normal bronchial epithelial cells, LKB1 coordinates with p114RhoGEF to regulate RhoA activity and maintain apical junctions (Xu *et al.*, 2010, 2013).

Complete LKB1 loss in a $Kras^{G12D}$-driven genetically engineered mouse model (GEMM) of lung cancer led to increased tumor burden, shortened survival time, and increased metastasis compared with $Kras^{G12D}$ mutant mice (Ji *et al.*, 2007). Despite these recent insights into LKB1 function, how LKB1 coordinates its kinase-dependent and -independent functions to regulate cell invasion remains poorly understood. Therefore we sought to uncouple defects in CTD function from defects in kinase function during cancer cell invasion. Our data show that the combination of defects in LKB1 kinase-dependent and -independent function creates a uniquely invasive cell that is unable to properly polarize and maintains an amoeboid shape; however, unlike classical amoeboid cells, LKB1-compromised cells maintain high focal adhesion kinase (FAK) activity and still remodel collagen during three-dimensional (3D) invasion. Our studies show that FAK-driven cell adhesion and collagen remodeling are caused by defective kinase activity, whereas amoeboid cell shape occurs due to RhoA signaling defects caused by a lack of LKB1 CTD farnesylation. Given that LKB1 frequently undergoes truncating mutations in lung adenocarcinomas that predictably affect both farnesylation and kinase activity, this highlights the importance of this potent combination of defects that could affect cancer cell metastasis.

RESULTS

LKB1 loss induces a morphological switch during 3D invasion to create a unique amoeboid cell population

To probe the role of LKB1 in regulating 3D invasion, we stably depleted LKB1 in H1299 non–small cell lung cancer cells (LKB1 wild type) and compared them with isogenic parental pLKO.1 vector control cells (Figure 1A). Stable knockdown of LKB1 resulted in cells switching from a mesenchymal morphology to an amoeboid morphology (Figure 1A). In the pLKO.1 cells, 47% of the invasive cells showed an amoeboid morphology, as compared with 73% in the shLKB1 cells. Mesenchymal cells were defined as cells that had a length greater than twice their width, as previously described (Nogawa and Mizuno, 1981; Ladhani *et al.*, 2011; Figure 1B). A similar transition was observed in H1792 cells (LKB1 wild-type NSCLC), with stable LKB1 depletion (Figure 1C). Similarly, a second LKB1-targeted short hairpin RNA (shRNA) in H1299 cells, as well as transient knockdown of LKB1 in H1299s and H1792s using small interfering RNA (siRNA), had similar effects, resulting in amoeboid-like morphology during invasion (Supplemental Figure S1). To confirm that this was an LKB1-dependent effect on cell invasion, we performed the reverse experiment and used H157 non–small cell lung cancer cells (LKB1-null) expressing either green fluorescent protein (GFP)–tagged full-length (wild type [WT]) LKB1 or empty GFP control vector to analyze invasive morphology. Reexpression of WT LKB1 caused invaded cells to switch from an amoeboid-like morphology to an elongated, mesenchymal-like morphology (Figure 1D). Of the invasive cells expressing LKB1, 61% of the cells were mesenchymal in morphology, as compared with 27% in the LKB1-null parental cells.

Live-cell imaging of H1299 pLKO.1 control and shLKB1 spheroids was performed to determine the percentage of amoeboid cells present in the total invasive population over time. These data confirm that LKB1 loss induces a switch to amoeboid morphology compared with control cells, and this switch was stable across all time points measured (Figure 1E). Single-cell-track plots show that LKB1-depleted amoeboid cells move greater distances from their point of origin than do mesenchymal cells found in the LKB1-depleted population and even other amoeboid cells found in pLKO.1 control cells (Figure 1F, bottom right). Whereas no difference in cell directionality was seen with LKB1 loss as measured by meandering index (Figure 1G, left), LKB1-depleted amoeboid cells show significantly increased velocity compared with all other cell types (Figure 1G, right), including amoeboid cells found in LKB1 wild-type pLKO.1 controls. These data suggest that amoeboid cell morphology alone cannot solely explain the increase in velocity and distance from the origin observed in the LKB1-depleted amoeboid cells.

The LKB1 C-terminal domain, and specifically its farnesylation, regulates cellular polarity and directional persistence

Because the majority of LKB1 mutations in lung cancer patients are truncations (Cancer Genome Atlas Research Network, 2014; Figure 2A), we made a series of stable cells reexpressing GFP-tagged LKB1 mutants and domain truncates (Figure 2, B and C) to determine whether they could induce mesenchymal invasion in both H157 LKB1-null human lung cancer cells and HeLa (LKB1-null cervical cancer) cells. Based on the use of 3D invasion assays of spheroids embedded in collagen, a full-length, wild type LKB1 induced mesenchymal polarization during invasion as compared with empty GFP control (Figure 2, D and E, and Supplemental Figure S2), confirming the data seen with the transient transfections (Figure 1D). Similarly, H157 cells reexpressing an LKB1 K78I kinase-dead mutant (Supplemental Figure S3) also exhibited mesenchymal polarity, indicating that kinase activity is not required for promoting mesenchymal polarization. In contrast, a C430S farnesylation mutant or a K78I and C430S double mutant was unable to significantly restore mesenchymal polarization over empty GFP control, highlighting the role of LKB1 farnesylation in promoting mesenchymal polarization during invasion in a kinase-independent manner.

We then tested the hypothesis that the C-terminal domain of LKB1 alone can restore mesenchymal polarization during invasion, since this contains the C430 farnesylation site. The LKB1 CTD alone is sufficient to promote mesenchymal polarization, highlighting kinase-independent promotion of mesenchymal polarity. Furthermore, mutation of the C430 site abolishes the ability of the CTD to

promote mesenchymal polarity in both H157 and HeLa cells (Figure 2, D and E, and Supplemental Figure S2). In addition, the LKB1 N-terminal domain (NTD) alone and kinase-domain alone both are unable to promote this mesenchymal polarization during invasion (Supplemental Figure S4). Overall these data suggest that the LKB1 C-terminal domain, and specifically its farnesylation, promotes mesenchymal polarity during invasion, and, of importance, this occurs independently of LKB1 kinase activity.

Our data show that the CTD and farnesylation promote mesenchymal polarization during invasion. Therefore we examined the role of LKB1 in regulating directional migration. Full-length wild-type LKB1, the LKB1 K78I kinase-dead mutant, and the LKB1 CTD alone significantly restore directional persistence over empty GFP control (Figure 2, F and G). On mutation of the C430 farnesylation site in wild-type LKB1, LKB1 K78I, and the LKB1 CTD, there is abrogation of directional persistence compared with their respective wild-type farnesylation constructs. Taken together, these data highlight the importance of LKB1 farnesylation, independent of its kinase activity, and specifically the CTD in regulating directed cell invasion.

LKB1 differentially regulates Rho-GTPases through its CTD and farnesylation

We next sought to understand the mechanism by which LKB1 regulates this amoeboid–mesenchymal invasion switch. Because amoeboid invasive motility is driven through a balance of RhoA and cdc42 activity (Huang *et al.*, 1997; Parri and Chiarugi, 2010; Morley *et al.*, 2014), we probed the activity of these GTPases in 3D spheroids. A time course of H1299 (wild-type LKB1) pLKO.1 control cells shows robust activation of both RhoA and cdc42 at the 5-h time point (Figure 3, A–D); however, the isogenic shLKB1 cells have reduced active cdc42 and RhoA. To enrich for motile cells, GTPase activation assays were performed in two dimensions. The data show that H1299 cells activate both RhoA and cdc42, but this activation is severely attenuated upon LKB1 loss (Figure 3, E–H). These data are consistent with previous reports showing that LKB1 depletion reduces cdc42 and RhoA activity in motile cells (Zhang *et al.*, 2008; Xu *et al.*, 2010, 2013) and suggest that LKB1-depleted cells do not rely on canonical Rho-GTPase activity.

Because the LKB1 CTD, and specifically its farnesylation, is critical for promoting mesenchymal motility, we examined the role of these domains in regulating Rho-GTPase activity. RhoA activity is enhanced upon reexpression of wild-type LKB1 relative to the empty GFP control (Figure 3, I and J), confirming that LKB1 is responsible for promoting RhoA activity. Similarly, the LKB1 CTD alone is sufficient for promoting RhoA activity, although inhibiting LKB1 farnesylation within the CTD completely abrogates RhoA activation (Figure 3, I and J). Taken together, these data suggest that LKB1 regulates RhoA activity through its CTD and specifically through its farnesylation.

The role of LKB1 in regulating cdc42 activity was then probed further because we previously showed that depletion of LKB1 affects cdc42 in human lung cancer cell lines in two dimensions (Zhang *et al.*, 2008). We found that wild-type LKB1 promotes cdc42 activity and that this occurs through the LKB1 CTD (Figure 3, K and L). Of interest, LKB1 farnesylation has no effect on the activity of cdc42, as the full-length farnesylation mutant is able to activate cdc42 at levels similar to those for wild-type LKB1. These data suggest that whereas LKB1 regulates cdc42 activity through its C-terminal domain, this activation is farnesylation-independent, unlike the farnesylation-dependent activation of RhoA (Figure 3, K and L).

LKB1 farnesylation activates RhoA to promote mesenchymal polarity

The present data show that LKB1 CTD, and specifically its farnesylation, promotes both mesenchymal cell polarity and RhoA activity. We next sought to determine whether LKB1 promotes mesenchymal polarization through RhoA signaling. We created double stable cells expressing either empty GFP or GFP-LKB1 wild type or a C430S farnesylation mutant and the constitutively active form of either RhoA (Q63L) or cdc42 (Q61L) (Figure 4A). Cells reexpressing wild-type LKB1 and either constitutively active RhoA or cdc42 maintain a mesenchymal polarization similar to cells reexpressing wild-type LKB1 alone (Figure 4, B and C). Similarly, rescuing cdc42 activity in farnesylation-mutant cells results in a predominantly amoeboid phenotype, similar to LKB1 farnesylation-mutant cells alone (Figure 4, B and C), suggesting that LKB1 does not signal to cdc42 to promote mesenchymal polarization. However, upon rescuing RhoA activity in LKB1 farnesylation-mutant cells, cells reacquire a mesenchymal polarization during 3D invasion (Figure 4, B and C). Of importance, this result is consistent with mesenchymal polarization in cells reexpressing wild-type LKB1. Restoring either RhoA or cdc42 activity in empty GFP control cells fails to restore this mesenchymal polarization (Figure 4, B and C). Given that our previous data highlight the role of LKB1 farnesylation in promoting mesenchymal polarity, these data suggest that this occurs through LKB1 signaling to RhoA, as rescuing RhoA activity in farnesylation-compromised cells restores mesenchymal polarity.

These results were expanded by examining directional migration in these cells expressing constitutively active RhoA or cdc42. Similar to cells reexpressing wild-type LKB1, cells reexpressing constitutively active RhoA or cdc42 maintain a strong directional persistence (Figure 4, D and E). In addition, cells reexpressing constitutively active cdc42 in LKB1 farnesylation-mutant cells have poor directional persistence, similar to farnesylation-mutant cells alone, suggesting that cdc42 signaling is not responsible for promoting directionality. However, on rescue of RhoA activity in these farnesylation-compromised cells, cells restore their directional persistence, similar to cells reexpressing wild-type LKB1 (Figure 4, D and E). Similar to mesenchymal polarization, restoring RhoA or cdc42 activity in empty GFP control cells fails to restore directional persistence. Taken together, these data highlight an LKB1 farnesylation-RhoA pathway that promotes mesenchymal polarity and strong directional persistence during 3D invasion.

The regulation of FAK activity by LKB1 is kinase dependent

The present data show that the LKB1 CTD is responsible for controlling the amoeboid–mesenchymal switch during 3D invasion. We and others have also shown that LKB1 loss results in an increase in adhesion signaling, most notably through hyperactive FAK signaling (Ji *et al.*, 2007; Carretero *et al.*, 2010; Kline *et al.*, 2013; Goodwin *et al.*, 2014). Thus we sought to determine whether this amoeboid–mesenchymal switch is related to adhesion signaling by using our panel of H157 stable cells (Figure 2B) to assess pFAK^{397} activity. We found, using immunofluorescence, that compared to empty GFP control cells, H157 cells expressing wild-type LKB1 showed repression of the total number of pFAK^{397} sites (Figure 5, A and B). This result is consistent with previous findings that LKB1 is a pFAK repressor in lung cancer cells (Kline *et al.*, 2013; Goodwin *et al.*, 2014). Of interest, this repression was not dependent on LKB1 farnesylation, as mutation of the LKB1 C430 farnesylation motif had no effect on the ability of LKB1 to repress pFAK^{397} (Figure 5, A and B). In contrast, on reexpression of either the K78I kinase-dead mutant or the K78I-C430S double mutant LKB1, pFAK^{397} expression was not

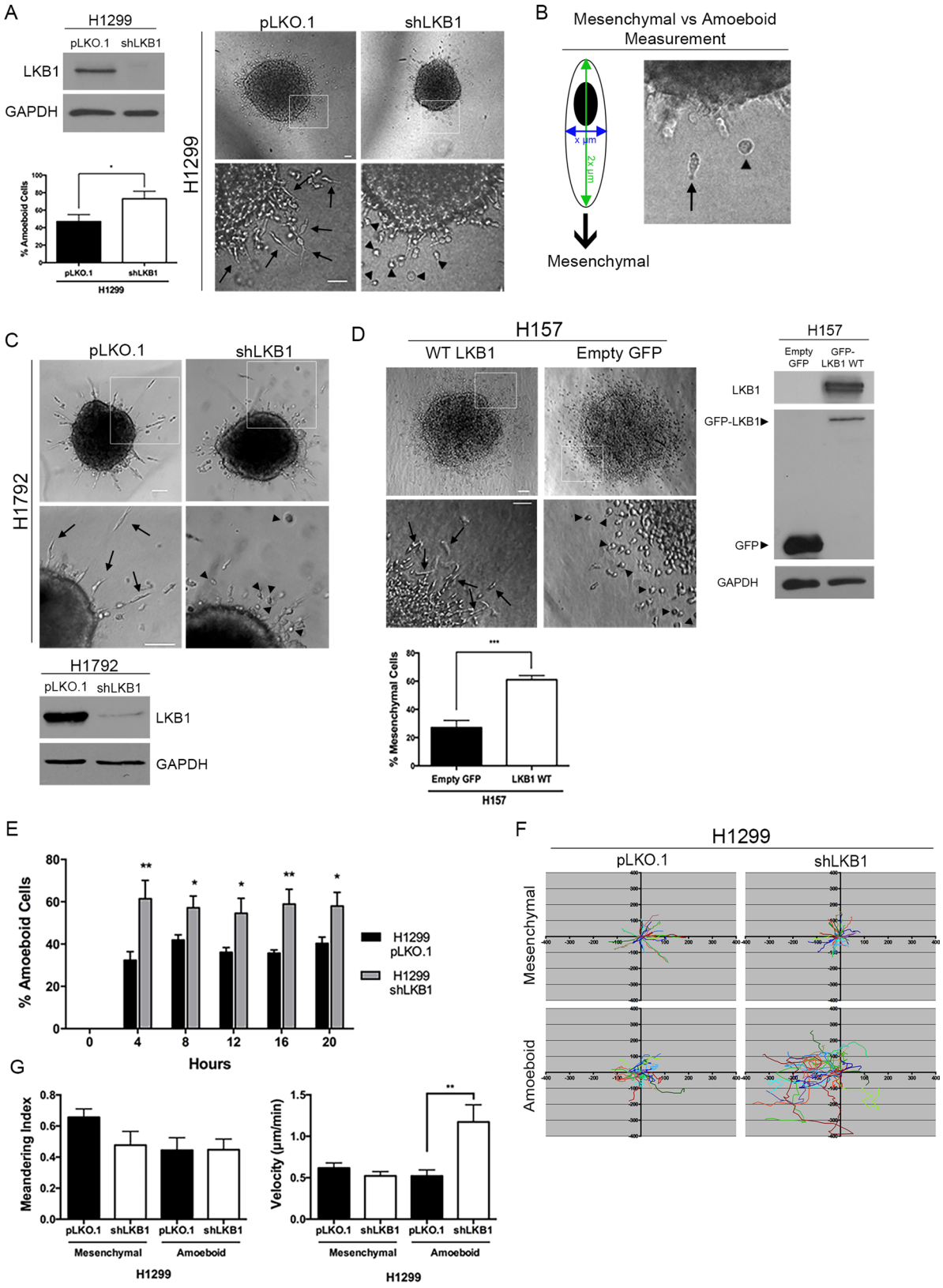

FIGURE 1: LKB1 induces a mesenchymal–amoeboid switch in 3D invasive morphology. (A) Western blot (left) showing that H1299 cells were stably depleted of LKB1 using a targeting shRNA lentivirus. Empty pLKO.1 vector was used as a control. Spheroids from H1299 pLKO.1 and shLKB1 cells were embedded in a collagen type I matrix and imaged at 24 h postembedding (right). Bottom, zoomed images. Amoeboid and mesenchymal cell morphologies were quantified as a percentage back to the total number of cells invaded in each spheroid. Three spheroids. Scale, 50 µm. Arrows, mesenchymal cells; arrowheads, amoeboid cells. (B) Schematic illustration of how mesenchymal and amoeboid cells were quantified. Any cell whose length was greater than or equal to twice its width was considered a

repressed and remained at levels similar to those for empty GFP control cells (Figure 5, A and B). Whereas LKB1 served to repress the total number of pFAK^{397} sites per cell, the mean intensity of each pFAK site was similar across all cell lines (Supplemental Figure S5). These data suggest that the kinase activity of LKB1, but not farnesylation, is necessary for LKB1 to repress FAK during 3D invasion.

To probe further the mechanism by which LKB1 regulates FAK, we analyzed the role of the downstream target of LKB1 kinase activity, MARK1, which represses FAK through an LKB1-MARK1 pathway (Goodwin *et al.*, 2014). Immunofluorescence staining of pFAK^{Y397} in MARK1 siRNA–depleted cells shows that MARK1 loss increases pFAK expression compared with scrambled siRNA control (Figure 5C), thus phenocopying the loss of LKB1. Quantification of pFAK^{Y397} staining confirms that MARK1 loss increases the number of pFAK sites per cell (Figure 5D), with a slight increase in the intensity of each pFAK site (Supplemental Figure S5). Western blot analysis of three LKB1 wild-type lung cancer lines (H1792, H1299, and H157 + GFP-LKB1) also shows an increase in pFAK^{Y397} with MARK1 knockdown (Figure 5E); however, MARK1 knockdown had no significant effect on cell morphology (Supplemental Figure S6), which is consistent with our data indicating that cell polarity during 3D invasion is independent of its kinase function.

LKB1-depleted amoeboid cells require FAK activation to navigate through a collagen matrix

We next wanted to determine the effect of LKB1 loss specifically on the amoeboid population because these cells showed a significant increase in velocity during invasion, even more so than amoeboid cells in the wild-type population (Figure 1F). We first assessed whether FAK was hyperactive in LKB1-depleted cells. Western blot confirmed an increase in pFAK^{Y397} in H1299 and H1792 LKB1-depleted cells compared with controls (Figure 6A); however, this provided information only on the whole population. Therefore we then analyzed single invasive cells for their pFAK status based on morphology in H1299 pLKO.1 and shLKB1 spheroids via immunofluorescence. We confirmed that LKB1 loss resulted in pFAK^{Y397} hyperactivation compared with pLKO.1 control cells (Figure 6B). The mean intensity of each individual pFAK site increased significantly from 748 in pLKO.1 cells to 1751 in shLKB1 cells (Figure 6C, left), and the total number of pFAK sites per cell showed a significant increase from 3 to 72 sites/cell with LKB1 depletion (Figure 6C, right). This increase in pFAK^{Y397} also resulted in increased downstream adhesion signaling, since both the mean phospho-paxillin (pPax^{Y118}) site intensity and total number of pPax^{Y118} sites per cell significantly increased (Figure 6, D and E).

We next examined pFAK^{Y397} expression specifically in mesenchymal and amoeboid cells of pLKO.1 and shLKB1 cells to determine whether shLKB1 amoeboid cells have unique FAK activity compared with wild-type LKB1 amoeboid cells. These data show that LKB1 loss increases pFAK^{Y397} expression in both mesenchymal and amoeboid cells that lack LKB1 (Figure 6F); however, the amoeboid populations within shLKB1 cells express significantly higher levels of pFAK compared with amoeboid cells in pLKO.1 control cells (Figure 6F), showing that this pFAK activity does not arise solely from amoeboid morphology.

To further probe this finding, we tested the hypothesis that inhibition of FAK activity will specifically inhibit shLKB1 amoeboid cell invasion due to the aberrantly active pFAK^{Y397} levels. We first transiently knocked down FAK via targeted siRNA and found that FAK knockdown completely abolished invasion in the H1299 shLKB1 cells (Supplemental Figure S6). To address how FAK activity alters cell morphology and motility specifically in LKB1-depleted cells, we pharmacologically inhibited FAK. H1299 pLKO.1 and shLKB1 spheroids were exposed to 1 μM FAK inhibitor PF-573228 and assayed for invasion over time using live-cell imaging. Inhibition of FAK did result in a significant decrease in the total shLKB1 cells invaded compared with dimethyl sulfoxide (DMSO) control, decreasing from ~65 to 35 cells/spheroid after 16 h of invasion (Figure 6G). In contrast, the FAK inhibitor had no significant effect on the total cells invaded in pLKO.1 spheroids (Figure 6G), suggesting that these cells are less dependent on adhesion during invasion. Of importance, using 1 μM FAK inhibitor did not completely abolish invasion in the shLKB1 cells, as siRNA treatment did, thus allowing for further analysis of cell motility features in the presence of inhibitor. Of interest, it was specifically the velocity of LKB1-depleted amoeboid cells that was significantly inhibited by exposure to FAK inhibitor (Figure 6H). The velocity of shLKB1 amoeboid cells in the presence of PF-573228 was equivalent to the velocity of pLKO.1 amoeboid cells, suggesting that increased FAK activity provides LKB1-depleted amoeboid cells an advantage of faster motility during invasion. In addition, whereas FAK inhibition specifically affects the velocity of shLKB1 amoeboid cells, it had no significant effect on cell shape (Figure 6I). These data taken together suggest that amoeboid cells lacking LKB1 expression represent an atypical population of rounded cells that use adhesion signaling for invasion through the collagen gel.

LKB1 loss causes an increase in collagen remodeling during 3D invasion

Because we found that LKB1 loss results in a unique amoeboid cell population, we wanted to determine whether this provides an invasive advantage while navigating the microenvironment. To do this, we performed multiphoton imaging on H1299 pLKO.1 and shLKB1 spheroids to visualize collagen remodeling and its relationship to cell type and invasive potential. LKB1 loss resulted in an increase in collagen alignment at 6 and 21 h (Figure 7A). We used a novel local alignment coefficient to quantify the heterogeneous alignment patterns. We used curvelet transform fiber extraction (CT-FIRE) software to extract collagen fibers (Figure 7B, i and ii). All fibers were quantized with a 5-pixel length. Then, for every pixel, we measured the

mesenchymal cell. Right, examples of each cell morphology. Arrow, mesenchymal cell; arrowhead, amoeboid cell. (C) Experiment from A repeated in H1792 NSCLC cells. Bottom, Western blot confirming LKB1 knockdown. (D) H157 cells (LKB1-null) were transiently transfected with either empty pcDNA3-GFP or pEGFP-C1 LKB1 WT vector. Spheroids were analyzed at 24 h for invasive phenotypes. Western blot confirms expression of GFP-LKB1 (right). Bottom, bar graph showing the percentage of mesenchymal cells in empty GFP control and LKB1-transfected H157 cells. (E–G) H1299 pLKO.1 and shLKB1 spheroids were embedded in a collagen matrix and imaged using live-cell confocal. (E) Bar graph showing the percentage of amoeboid cells calculated over time in H1299 pLKO.1 and shLKB1 cells. Eight spheroids. (F) Cell tracks were plotted from a single point of origin in H1299 pLKO.1 and shLKB1 invasive amoeboid and mesenchymal cells. (G) Bar graph showing meandering index and velocity of H1299 shLKB1 and pLKO.1 subtypes; 11 cells. *$p \leq 0.05$, **$p \leq 0.01$, and ***$p < 0.001$.

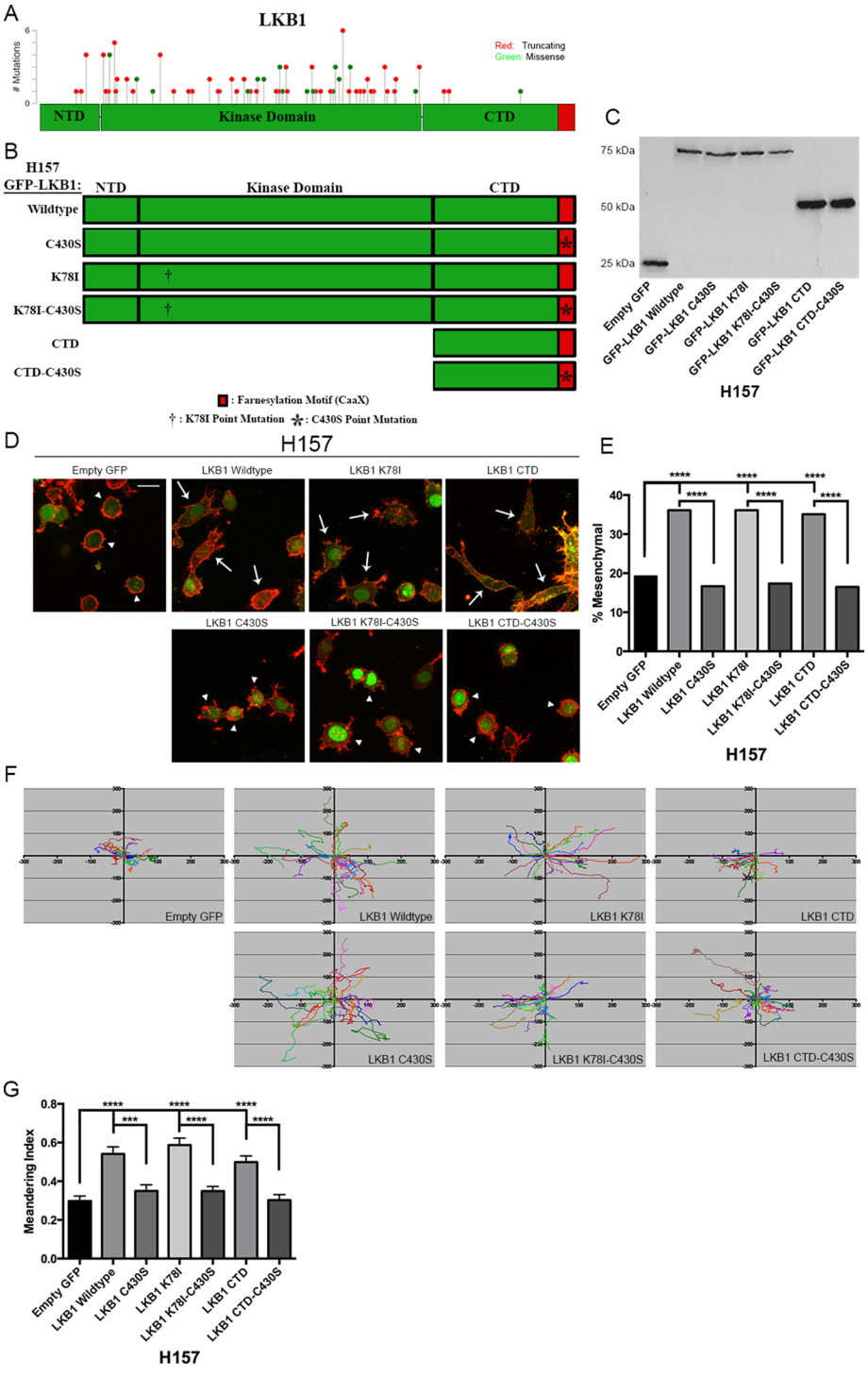

FIGURE 2: LKB1 regulates cellular polarization through its C-terminal domain in a farnesylation-dependent manner. (A) LKB1 consists of a central kinase domain with a C-terminal farnesylation motif. Schematic of LKB1 mutations in lung adenocarcinoma patients; data adapted from cBioPortal (www.cbioportal.org). Red, truncating mutations; green, missense. (B) Schematic showing H157 (NSCLC, LKB1-null) cells that were generated stably expressing GFP-tagged, wild-type LKB1, a C430S mutation to disrupt farnesylation, a K78I kinase-dead mutation, a double mutation with both K78I and C430S, the CTD alone, or the CTD alone with a C430S mutation. (C) Western blot probed with a GFP antibody verifying expression of the H157 stable cells. (D) Immunofluorescence of H157 spheroids embedded in collagen and stained with phalloidin. Amoeboid and mesenchymal morphologies (described in Figure 1) were quantified as a percentage back to the total number of cells invaded in each spheroid. Four spheroids. Scale, 20 μm. Arrows, mesenchymal cells; arrowheads, amoeboid cells. (E) The percentage of mesenchymal cells was quantified for each cell line at 24 h postembedding. (F) Each cell line was tracked over time. Cell tracks were plotted from a single point of origin. (G) Meandering index (defined as the linear distance divided by the total path length) was calculated using the cell tracks from F; 30 cells. ***$p \leq 0.001$ and ****$p \leq 0.0001$.

local alignment coefficient parameter for every pixel by selecting all fiber segments within a circular neighborhood of 20 pixels (Figure 7Biii) to generate the alignment field (Supplemental Figure S7 explains the optimization of the local alignment coefficient calculation). Using this parameter, we generated histograms of local alignment coefficients, surface plots, and contour plots to quantify alignment (Figure 7C). Using this quantification of the local alignment coefficient and comparing to the 0-h baseline value, we found that at 6 h, shLKB1 cells show an increase in collagen alignment, which is further accentuated at 21 h; on the other hand, pLKO.1 control cells show in a decrease in the number of aligned fibers over time (Figure 7D), suggesting that LKB1 might actually negatively regulate remodeling during invasion. Thus LKB1-depleted cells are more efficient at realigning collagen fibers as they invade. Of interest, this realignment of the collagen matrix seems to occur via a matrix metalloproteinase (MMP)–independent mechanism. When treated with the pan-MMP inhibitor GM6001, shLKB1 showed no significant change in invasion compared with vehicle control (Supplemental Figure S8). These data suggest that LKB1 loss promotes collagen remodeling in an MMP-independent manner.

LKB1 kinase activity represses collagen remodeling through regulation of FAK activity

We next wanted to test the hypothesis that LKB1 kinase activity represses collagen remodeling. Therefore we assessed collagen remodeling and invasion in H157 cells stably expressing various LKB1 domains or mutants. At 24 h, H157 empty GFP–invading cells show epicenters of significant collagen alignment (Figure 8Ai), whereas cells expressing either LKB1 wild type or LKB1 C430S show significantly less alignment (Figure 8A, ii and iii). However, cells expressing either the K78I kinase-dead LKB1 or the K78I-C430S double mutant LKB1 fail to repress alignment (Figure 8A, iv and v), suggesting that kinase activity is required for collagen remodeling. Quantification of alignment shows that empty GFP, LKB1 K78I, and LKB1 K78I-C430S cells have

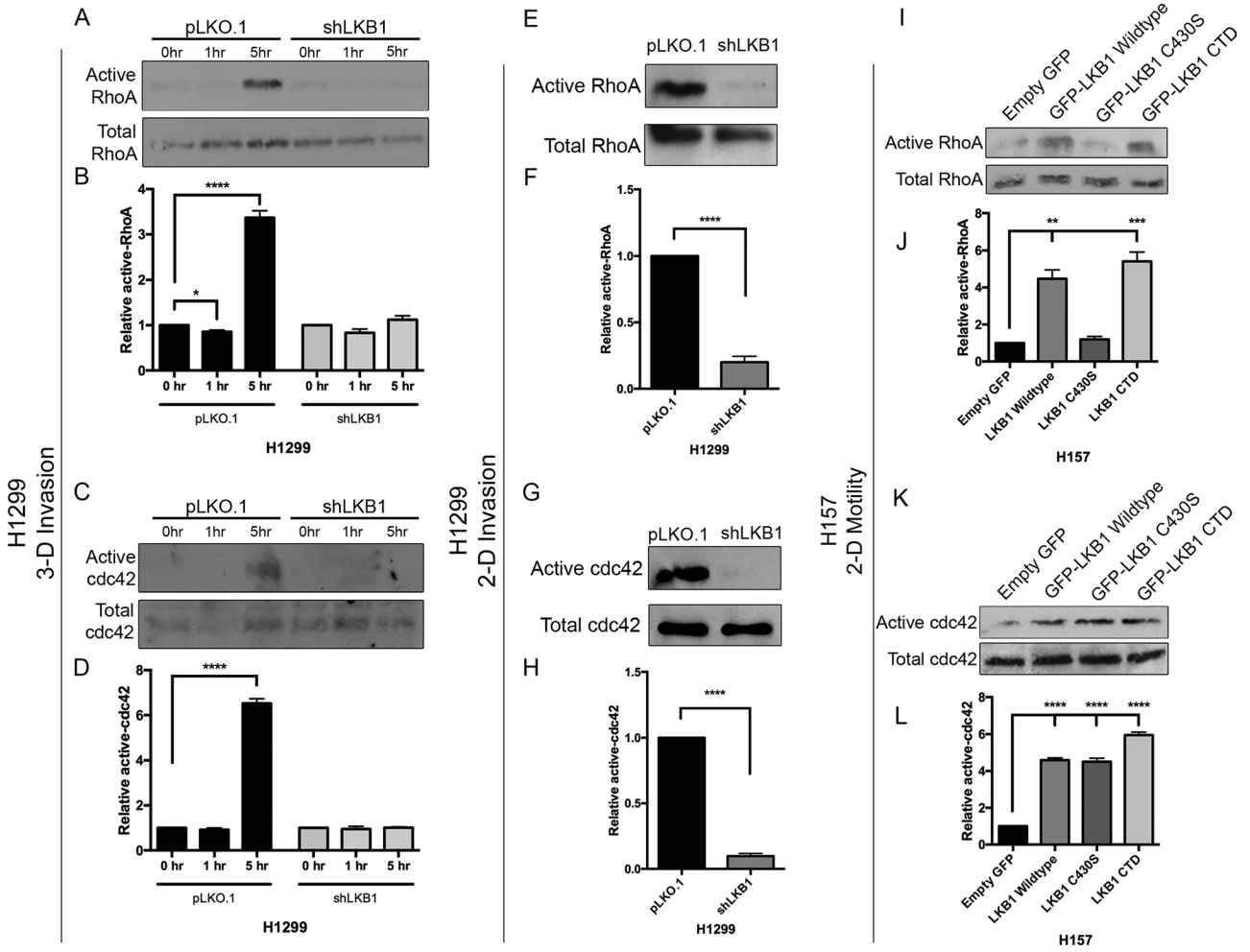

FIGURE 3: LKB1 differentially regulates RhoA and cdc42. (A) Representative Western blot showing RhoA activity assay over time in pLKO.1 and shLKB1 H1299 cells embedded in a collagen type I matrix. (B) Densitometry of Western blot from A normalized to total RhoA levels. (C) Representative Western blot of a cdc42 activity assay over time in pLKO.1 and shLKB1 H1299 cells embedded in a collagen type I matrix. (D) Densitometry of Western blot from C normalized to total cdc42 levels. (E) Representative Western blot showing RhoA activity assay in two dimensions in pLKO.1 and shLKB1 H1299 cells. (F) Densitometry of Western blot from E normalized to total RhoA levels. (G) Representative Western blot showing cdc42 activity assay in two dimensions in pLKO.1 and shLKB1 H1299 cells. (H) Densitometry of Western blot from G normalized to total cdc42 levels. (I) Representative RhoA activity assay of H157 cells stably expressing either empty GFP control or GFP-tagged, wild-type LKB1, LKB1 C430S, or the LKB1 C-terminal domain. (J) Densitometry of Western blot from I normalized to total RhoA levels. (K) Representative Western blot showing a cdc42 activity assay of H157 cells stably expressing either empty GFP control or GFP-tagged, wild-type LKB1, LKB1 C430S, or the LKB1 C-terminal domain. (L) Densitometry of Western blot from K normalized to total cdc42. Three experiments. *$p \leq 0.05$, **$p \leq 0.01$, ***$p \leq 0.001$, and ****$p \leq 0.0001$.

increased alignment coefficients compared with those cells expressing LKB1 wild type or C430S (Figure 8B).

We then transiently knocked down MARK1 via siRNA in H157 LKB1 wild-type cells to determine whether LKB1 kinase activity signals through MARK1 to repress FAK activity. Cells lacking MARK1 phenocopy LKB1-depleted cells, showing increased remodeling compared with scrambled siRNA control (Figure 8C). This remodeling can be inhibited by treating H1299 shLKB1 cells with PF-573228 FAK inhibitor (Supplemental Figure S8), supporting the concept that FAK activity is required for the increase in manipulation of the collagen gel. These data point to the LKB1-MARK1-FAK pathway for regulating collagen remodeling as cells invade.

We next reasoned that since the LKB1-depleted amoeboid cells have high levels of FAK activity, even compared with wild-type amoeboid cells, perhaps these cells also can remodel collagen. This would be unlike typical amoeboid cells, which in general do not remodel collagen (Wolf *et al.*, 2003a,b). To test this, we acquired images of single amoeboid cells within the H157 cells expressing different LKB1 domains and mutants. Surprisingly, H157 empty GFP–invading amoeboid cells were associated with high collagen alignment (Figure 8D, arrows). In contrast, H157 amoeboid cells with wild-type LKB1 did not show local collagen alignment. The LKB1 K78I mutant was similar to the GFP control, indicating that LKB1 kinase activity is required to suppress local collagen alignment. Reexpression of the LKB1 C430S mutant was similar to LKB1 wild-type cells and showed no local alignment in amoeboid cells, again indicating that LKB1 kinase activity but not farnesylation is important for collagen remodeling. These data show that amoeboid cells lacking LKB1 kinase

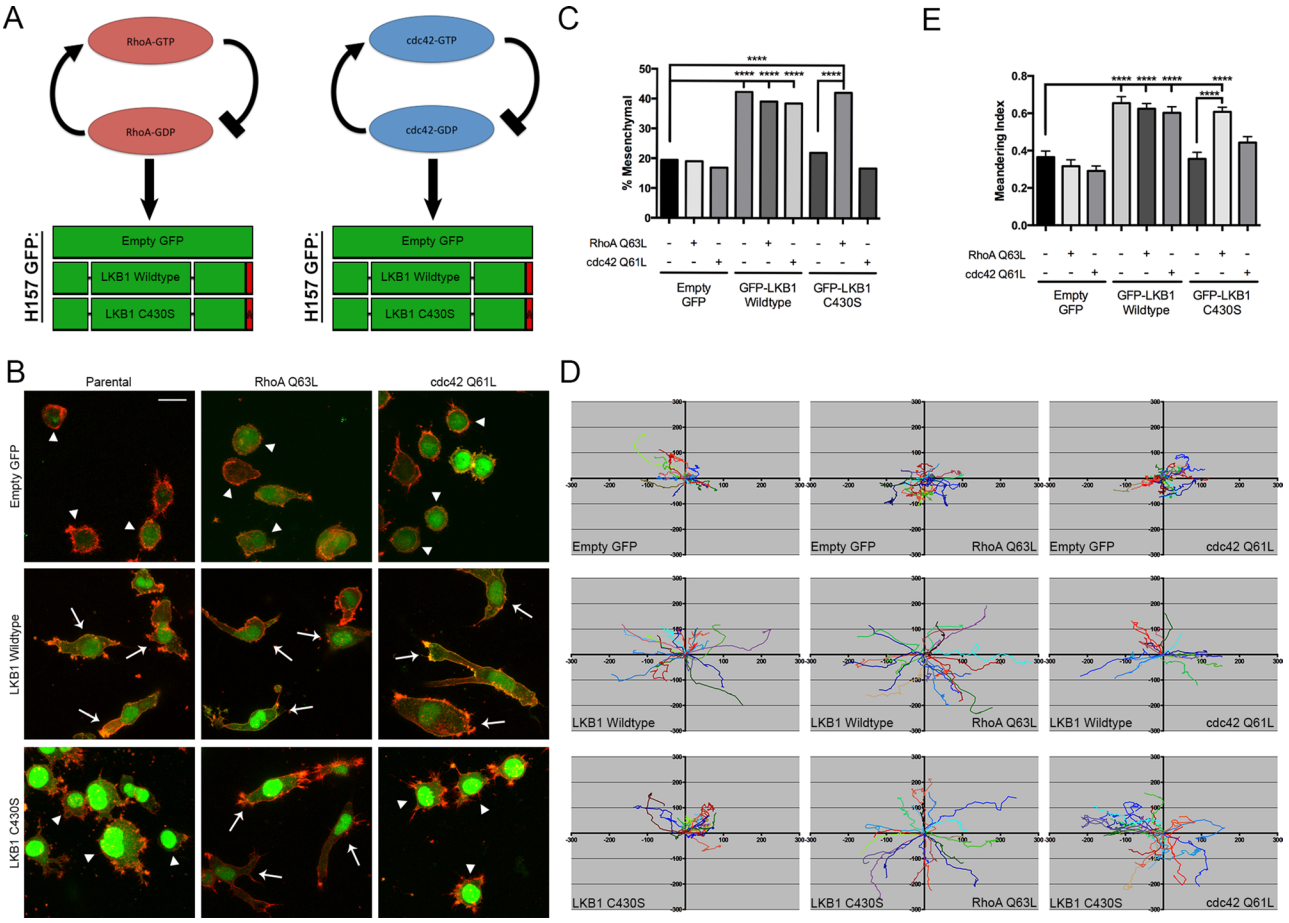

FIGURE 4: Constitutively active RhoA restores mesenchymal polarity in LKB1 farnesylation-mutant cells. (A) Schematic of double-stable cell lines expressing either empty GFP control or GFP-tagged, wild-type LKB1 or LKB1 C430S with constitutively active RhoA (Q63L) or cdc42 (Q61L). (B) Spheroids of H157 cells expressing either empty GFP control or GFP-tagged, wild-type LKB1 or LKB1 C430S and spheroids of these cells also expressing constitutively active RhoA or cdc42 were embedded in a collagen type I matrix. At 24 h postembedding, cells were fixed and stained with phalloidin. Amoeboid and mesenchymal morphologies (described in Figure 1) were quantified as a percentage back to the total number of cells invaded in each spheroid. Four spheroids. Scale, 20 μm. Arrows, mesenchymal cells; arrowheads, amoeboid cells. (C) The percentage of mesenchymal cells was quantified for each cell line at 24 h postembedding. (D) Each cell line was tracked over time. Cell tracks were plotted from a single point of origin. (E) Meandering index was calculated using the cell tracks from D. Meandering index is defined as the linear distance divided by the total path length; 30 cells. ****$p \leq 0.0001$.

activity boast the invasive advantage of remodeling a 3D collagen matrix, which does not typically occur in amoeboid motile cells.

DISCUSSION

The functional diversity of LKB1 has been attributed to it phosphorylating 14 members of the AMPK family of proteins, which, when activated, regulate a diverse set of biological processes (Lizcano *et al.*, 2004; Jaleel *et al.*, 2005;Hardie and Alessi, 2013). However, multiple reports show a kinase-independent function of LKB1 that is linked to cell polarity (Lo *et al.*, 2012; Nakano and Takashima, 2012). Because a majority of the truncating mutations (Cancer Genome Atlas Research Network, 2014; ~72% of *LKB1* mutations in lung adenocarcinoma patients; Figure 2A) would predictably disrupt its kinase activity and remove its C-terminal domain, we sought to uncouple defects in CTD function from defects in kinase function in the context of cancer cell invasion. These results support an overall model in which the LKB1 CTD regulates cell polarization through a mesenchymal–amoeboid cell switch, whereas the kinase domain regulates FAK-based cell adhesion during invasion. These results suggest that when both kinase activity and CTD function are compromised, both aberrant cell polarity and adhesion programs ensue. Our data indicate that this is indeed the case; complete LKB1 depletion creates a uniquely invasive, amoeboid-shaped cell that, in contrast to typical amoeboid cells (Mandeville *et al.*, 1997; Friedl *et al.*, 1998; Friedl and Wolf, 2003), maintains a hyperactive FAK-based cell adhesion program and remodels collagen. We speculate that truncating mutations in *LKB1* mutant patients might create a similar scenario (Figure 9), in which both CTD and kinase function is disrupted, leading to increased invasiveness by creating an agile cell that can be amoeboid, adherent, and able to navigate the tumor microenvironment.

Our results show that specifically LKB1 CTD farnesylation is required for proper polarization during invasion, such that when farnesylation is intact, cells are more mesenchymal, whereas cells revert to an amoeboid morphology upon its loss (Figure 3, D and E). This suggests that LKB1 membrane localization drives proper cell

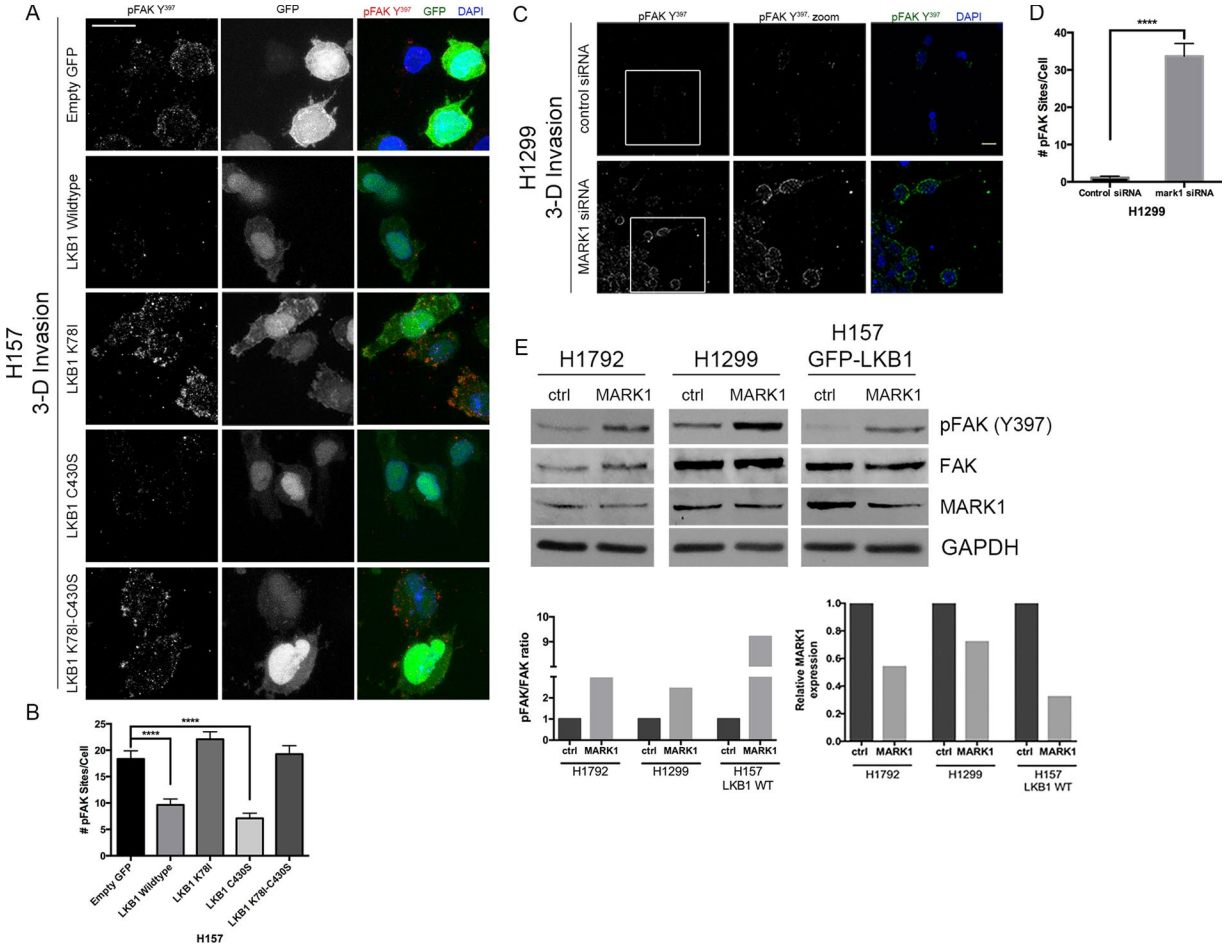

FIGURE 5: LKB1 regulates pFAK activity through its kinase domain. (A) Spheroids of H157 cells stably expressing either empty GFP control or GFP-tagged LKB1 constructs embedded in a collagen type I matrix. After 24 h, cells were fixed and stained by immunofluorescence for pFAK^{Y397}, GFP, and DAPI. (B) Total number of pFAK^{Y397} sites for each experimental group in A was quantified. (C) Expression of pFAK^{Y397} was examined by immunofluorescence of spheroids after 24 h of invasion. DAPI was used to stain the nuclei of the cells. (D) The total number of pFAK^{Y397} sites per cell was quantified from the images obtained in C. ****$p \leq 0.0001$. (E) Western blot showing pFAK^{Y397} expression after MARK1 siRNA depletion in H1792, H1299, and H157 LKB1 WT cells compared with scrambled control siRNA. GAPDH was used as a loading control. Bottom, densitometry analysis of phospho to total FAK ratio (left) and relative MARK1 expression (right) in control siRNA– and MARK1 siRNA–treated cells.

polarization and controls a mesenchymal–amoeboid morphological switch. Because LKB1 loss leads to inactivation of the small Rho-GTPases RhoA and cdc42 (Zhang *et al.*, 2008; Xu *et al.*, 2010, 2013; Figure 3, A–H), we followed up this observation and showed that whereas the LKB1 CTD alone is capable of activating both RhoA and cdc42, LKB1 farnesylation is critical only for the activation of RhoA (Figure 3, I–L), suggesting prenylation-independent regulation of cdc42. Similarly, a constitutively active RhoA, but not cdc42, can rescue mesenchymal polarization upon LKB1 farnesylation defects (Figure 4B), again supporting a role for RhoA but not cdc42 in promoting mesenchymal polarization. Of interest, it appears that a region of LKB1 is necessary to rescue polarity defects in these cells because restoring RhoA activity in empty GFP control cells fails to restore mesenchymal polarity. Previous studies showed that LKB1 regulates p114RhoGEF to promote RhoA activity (Xu *et al.*, 2013), and thus we propose that LKB1 CTD farnesylation anchors LKB1 into the membrane to promote this activity. It was unclear why LKB1 loss inactivates RhoA and cdc42 signaling (Zhang *et al.*, 2008; Xu *et al.*, 2010, 2013), since it would be expected that LKB1 loss, which causes increased invasion (Chan *et al.*, 2014; Li *et al.*, 2014), would instead hyperactivate RhoA and cdc42. However, recent studies show RhoA loss-of-function driver mutations in gastric cancer (Kakiuchi *et al.*, 2014; Wang *et al.*, 2014), suggesting that inactivation of RhoA, and perhaps cdc42, could in fact be a driver of tumor progression.

We show that LKB1 is a repressor of adhesion signaling and collagen remodeling in which intact kinase activity is required to maintain normal FAK levels (Figures 5–8). Restoration of LKB1 kinase activity in LKB1-deficient cells is sufficient to repress FAK-positive adhesion sites and collagen remodeling (Figure 5, A and B). Depletion of the LKB1 kinase target MARK1 is sufficient to phenocopy this (Figure 5, D and E), and these data are consistent with previous findings that highlight LKB1 as a FAK repressor (Carretero *et al.*, 2010; Kline *et al.*, 2013) through its kinase-dependent activation of MARK1 (Goodwin *et al.*, 2014), although our previous data also suggest that the LKB1 NTD alone can also repress FAK, suggesting a potential dual mechanism for interacting with and controlling FAK activity. Our data also build on the LKB1-MARK1 signaling pathway

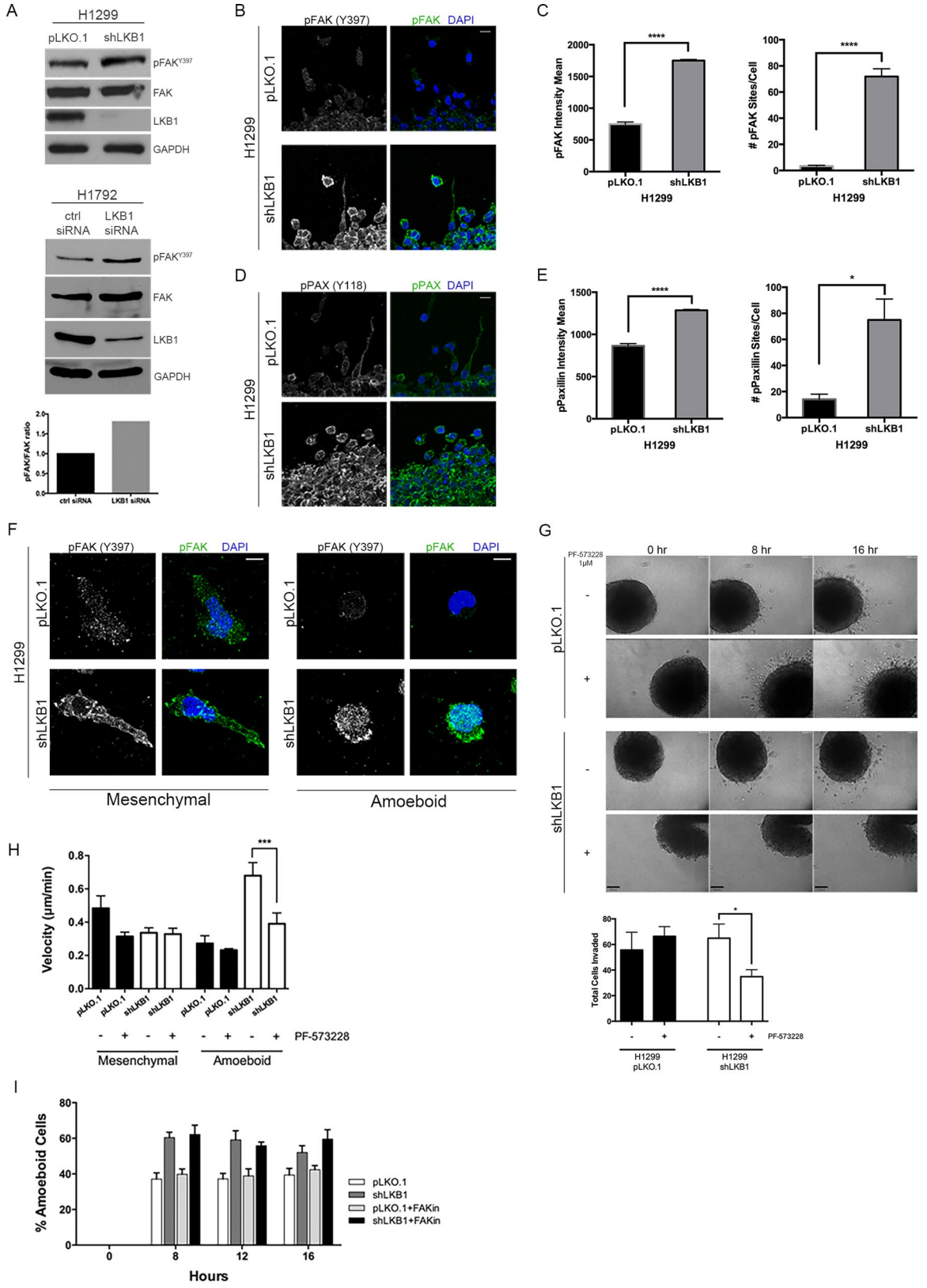

FIGURE 6: LKB1-depleted amoeboid cells depend on pFAK during invasion. (A) Western analysis of pFAK^{Y397} expression in H1299 pLKO.1 and shLKB1 cells (top). A similar experiment was performed in H1792 LKB1 siRNA treated cells (bottom). Bar graph shows densitometry of the phospho to total FAK ratio in the H1792 LKB1 knockdown cells compared with control siRNA. (B) H1299 pLKO.1 and shLKB1 spheroids were analyzed for expression of pFAK^{Y397} using IF imaging. Scale, 20 μm. (C) Quantification of pFAK^{Y397} site intensity (left) and total number of pFAK^{Y397} sites per cell (right). (D) Activity of downstream FAK signaling was analyzed using IF imaging of pPAX^{Y118} in H1299 pLKO.1 and shLKB1 spheroids. Scale, 20 μm. (E) Quantification of pPAX^{Y118} site intensity (left) and total number of pPAX^{Y118} sites per

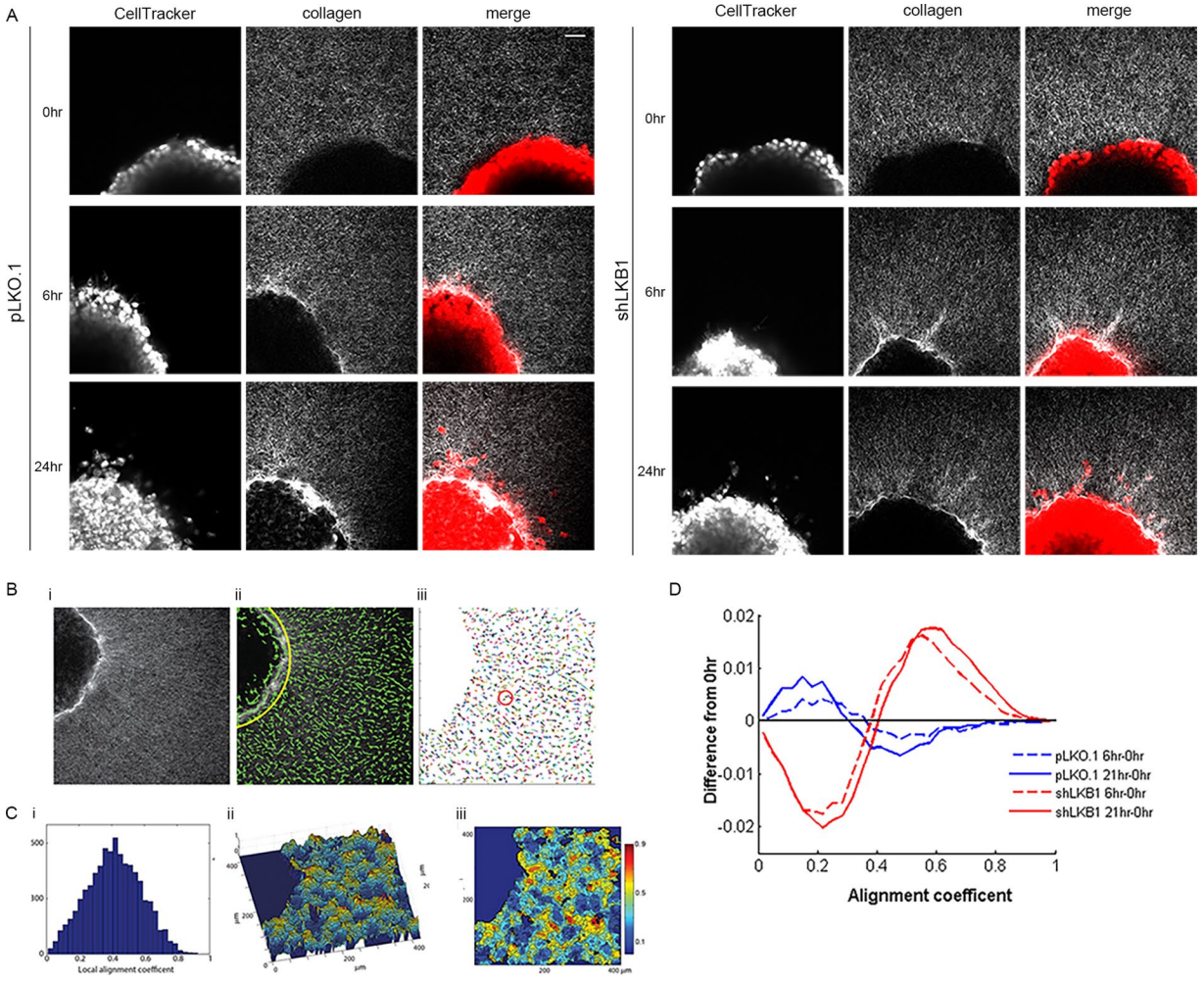

FIGURE 7: Loss of LKB1 results in increased collagen remodeling during invasion. (A) H1299 pLKO.1 and shLKB1 spheroids and the collagen matrix were imaged using SHG microscopy. Spheroids were dyed using CellTracker Red in order to visualize cells during invasion. Images were obtained at 0, 6, and 21 h postembedding. Scale, 50 μm. (B) Images from A were quantified using collagen alignment analysis. A single *z*-stack image (i) is used in CT-FIRE software to extract collagen fibers (green; ii). The software automatically determines various fiber lengths in the image, represented as different line colors (iii). A yellow line represents the manually selected tumor boundary. (C) i) Example histogram generated via CT-FIRE analysis of collagen alignment coefficients. ii) Surface and iii) contour plots of local alignment show topography of alignment patterns. (D) Alignment analysis was performed as described in B and C for H1299 pLKO.1 (blue) and shLKB1 (red) spheroids at 6 and 21 h, with the 0-h baseline alignment subtracted to remove any initial bias.

by showing that it regulates collagen remodeling during invasion in a FAK-dependent manner (Figure 8). LKB1 regulates lysyl oxidase (LOX), a collagen cross-linking enzyme, through the mTOR/HIF-1σ signaling pathway (Gao *et al.*, 2010), where LKB1 loss leads to increased LOX expression and collagen deposition (Gao *et al.*, 2010; Han *et al.*, 2014). Potentially, these two pathways are linked or related through FAK, since LOX is responsible for hypoxic human cancer cell invasion through FAK activity and cell–matrix adhesion (Erler *et al.*, 2006).

In contrast to classical amoeboid cell motility, LKB1-depleted amoeboid cells lack Rho-GTPase activity, have high FAK activity, and still remodel collagen (Figures 3 and 5–8). Classical amoeboid cells do not generally make sustained contacts with the extracellular matrix and do not remodel collagen fibers as they move; instead, their

cell (right). (F) Zoomed images of pFAK immunofluorescence imaging (described in B). Mesenchymal and amoeboid cell types in H1299 pLKO.1 and shLKB1. Scale, 10 μm. (G–I) H1299 pLKO.1 and shLKB1 spheroids were exposed to either 1 μM PF-573228 FAK inhibitor or vehicle control and imaged over time. (G) Still images of the live-cell imaging experiment were taken every 8 h. Bottom, quantification of total cells invaded, showing significantly decreased cells invaded in shLKB1 cells treated with FAK inhibitor. Scale, 100 μm. (H) Cell tracks from the FAK inhibitor experiment showed that LKB1-depleted amoeboid cells have a significantly decreased velocity during invasion compared with vehicle control; 8–15 cells. (I) The percentage of amoeboid cells in the live cell FAK inhibitor experiment was assessed at 0, 8, 12, and 16 h; five or six spheroids. *$p \leq 0.05$, ***$p \leq 0.001$, ****$p \leq 0.0001$.

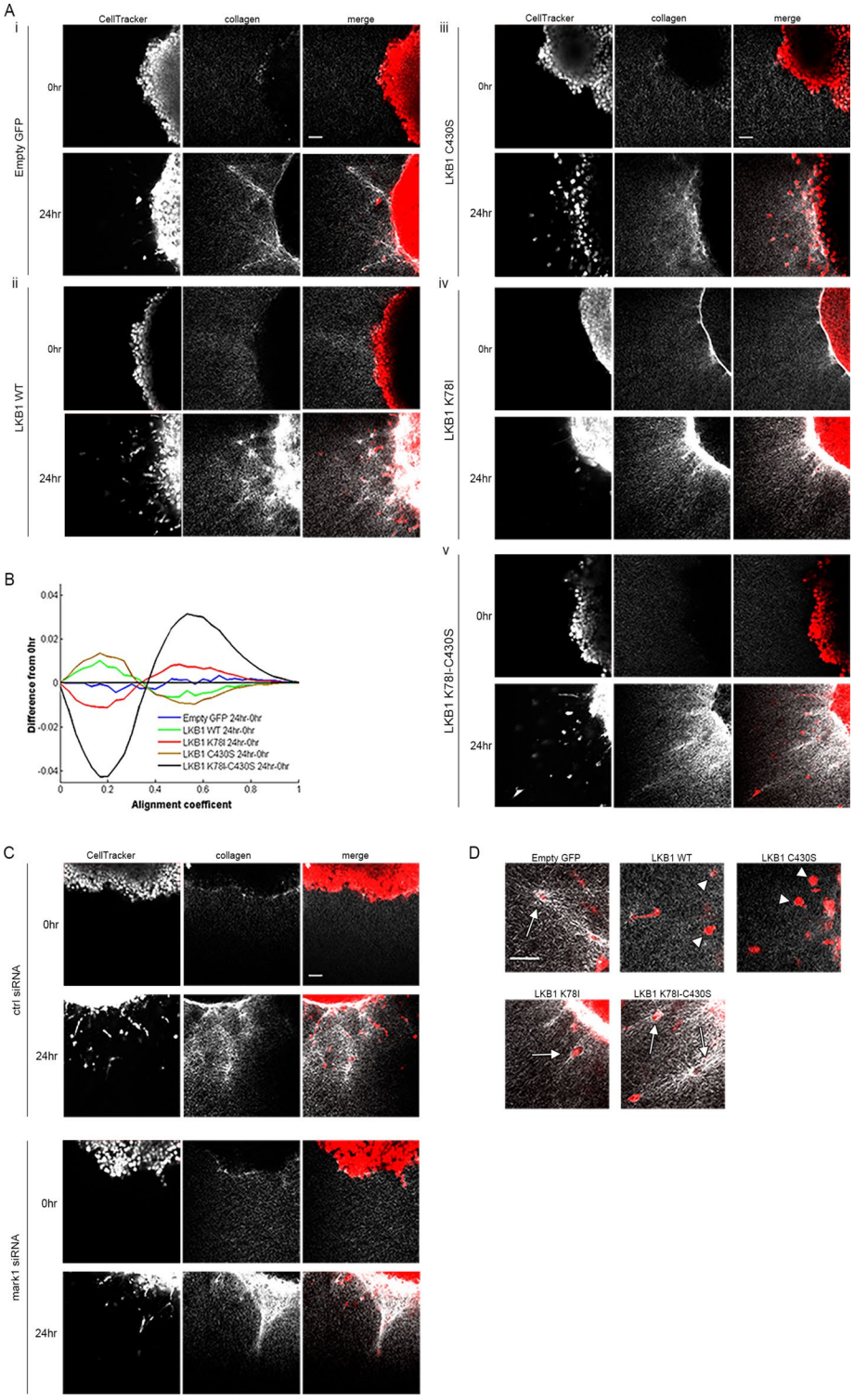

FIGURE 8: Kinase activity of LKB1 represses collagen remodeling. (A) Multiphoton imaging was performed at 0 and 24 h to visualize collagen using H157 stables with the following LKB1 constructs: empty GFP control, LKB1 WT, LKB1 C430S (farnesylation mutant), LKB1 K78I (kinase dead), and LKB1 K78I-C430S. (B) Images obtained in A were quantified for collagen alignment using CT-FIRE image analysis. (C) Collagen SHG imaging of MARK1 siRNA–depleted H157 LKB1 wild-type stable cells compared with scrambled siRNA. (D) Zoomed images showing collagen and single invading cells. Arrow, amoeboid cell that remodels collagen; arrowhead, amoeboid cell that does not remodel collagen. Scale, 50 μm.

motility depends on squeezing through and deforming the matrix during invasion (Haston *et al.*, 1982; Mandeville *et al.*, 1997; Friedl *et al.*, 1998; Friedl and Wolf, 2003; Wolf *et al.*, 2003a). In addition, RhoA is frequently implicated in amoeboid invasion by promoting Rho-associated coiled-coil kinase–mediated myosin light chain phosphorylation to promote actomyosin contractility required for cell blebbing during invasion (Sahai and Marshall, 2003; Wyckoff *et al.*, 2006; Gadea *et al.*, 2007; Rosel *et al.*, 2008; Kosla *et al.*, 2013). In contrast, amoeboid cells lacking LKB1 activity have reduced RhoA activity, and instead, restoring RhoA in LKB1-depleted cells promotes a mesenchymal, polarized cell (Figure 4, B and C). Therefore we propose that LKB1 inactivation in both its kinase domain and CTD disrupts cell polarity and adhesion signaling, resulting in a uniquely invasive cell that is adhesive, amoeboid in shape, and remodels collagen but might only represent an amoeboid cell in shape rather than the underlying molecular biology.

In vivo studies highlight the importance of LKB1 as a metastasis suppressor. In a seminal publication, LKB1 function was assessed using a *Kras*^{G12D}-driven GEMM of lung cancer (Ji *et al.*, 2007). In this model, *Lkb1* inactivation in mutant *Kras* tumors led to increased tumor burden, shortened survival time, and increased metastasis compared with *Kras* mutant–only mice. Furthermore, these mice had hyperactive FAK (Carretero *et al.*, 2010), similar to that described in our 3D model here. It is difficult to assess polarity during invasion in an in vivo model to determine whether these cells have polarity defects as well; however, future imaging of living lung tissue slices could shed light on this. In addition, given that LKB1 serves as the upstream regulator of AMPK in the energy stress response pathway (Shaw *et al.*, 2004), the interplay between defects in metabolic signaling, adhesion, and cell polarity remains unclear in the context of lung cancer metastasis.

Taken together, our data support a model in which LKB1 kinase–dependent and –independent functions have separate roles in regulating various cellular processes during cancer cell invasion, which when lost, synergize to create an uniquely invasive cell. Thus we speculate that loss of both LKB1 kinase activity and the CTD, which predictably occurs in lung adenocarcinoma patients with LKB1-truncating mutations, results in an aberrantly polarized and adhesive

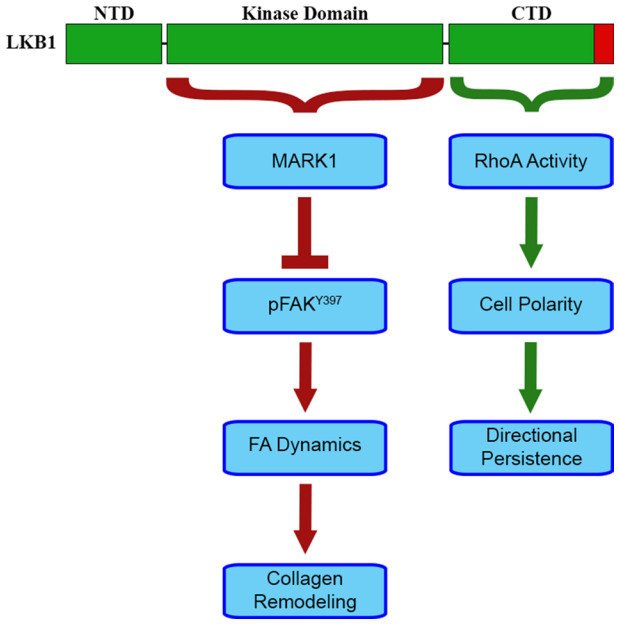

FIGURE 9: Model. LKB1 provides kinase-dependent and -independent mechanisms of regulating cell polarity during invasion. Through the LKB1 CTD and its farnesylation, LKB1 activates the Rho-GTPase RhoA to promote mesenchymal polarization and strong directional persistence during invasion. Independent of its CTD, LKB1 kinase activity phosphorylates MARK1 to repress the active form of focal adhesion kinase (pFAK), leading to regulation of focal adhesion dynamics and collagen remodeling during 3D invasion.

cell population that is superior at navigating the microenvironment during invasion.

MATERIALS AND METHODS

Cell culture and generation of stable cells

H1299, H1792, and H157 human NSCLC cells (American Type Culture Collection [ATCC], Manassas, VA) were cultured in RPMI-1640 medium supplemented with 10% fetal bovine serum and 100 U/ml penicillin/streptomycin and maintained at 37°C and 5% CO_2. HeLa human cervical cancer cells (ATCC) were cultured in DMEM supplemented with 10% fetal bovine serum and 100 U/mL penicillin/streptomycin and maintained at 37°C and 5% CO_2. Stable pLKO.1 vector control and LKB1-shRNA (shLKB1) H1299 and H1792 cells were created as previously described (Kline *et al.*, 2013). Briefly, these cells were created by lentiviral infection using specific shRNA constructs from Open Biosystems (Rockford, IL). Puromycin (2 µg/ml; Sigma-Aldrich, St. Louis, MO) was used to select transduced cells and Western analysis used to confirm knockdown.

To generate H157 and HeLa cells stably expressing LKB1 and constitutively active RhoA or cdc42, wild-type LKB1 and the various LKB1 domains and mutations were cloned into a pEGFP-C1 vector. Empty GFP or the GFP-LKB1 constructs were then subcloned from the pEGFP-C1 vector into a pBabe-puro vector. Constitutively active RhoA (Q63L) and cdc42 (Q61L) were subcloned from a pCDNA3 vector into pBabe-Hygro. The pBabe constructs were then transfected into Phoenix-ampho cells with Lipofectamine 2000 and PLUS reagent (Invitrogen, Grand Island, NY). Cells expressing only empty GFP or GFP-LKB1 were selected with 1 µg/ml puromycin, and cells coexpressing the constitutively active RhoA or cdc42 mutants were selected with 1 µg/ml puromycin and 300 µg/ml hygromycin (EMD Millipore, Billerica, MA). Proper expression of GFP-LKB1 was verified using immunofluorescence (IF) and Western blot to confirm phenotype and molecular weight. Expression of constitutively active RhoA and cdc42 was confirmed using a Rho-GTPase activity assay comparing the constitutively active mutants to their isogenic partner lines.

Antibodies and stains

Antibodies were used against pFAK^{Y397}, pPaxillin^{Y118}, MARK1, glyceraldehyde-3-phosphate dehydrogenase (GAPDH), GFP (Cell Signaling, Boston, MA), LKB1 (Santa Cruz Biotechnology, Santa Cruz, CA), RhoA, and cdc42 (Cytoskeleton, Denver, CO) for 3D immunofluorescence, Western blotting, and immunoprecipitation. Alexa Fluor 555–phalloidin, Alexa Fluor 488, and Alexa Fluor 555 goat-anti-rabbit (Invitrogen) and 4′,6-diamidino-2-phenylindole (DAPI; Invitrogen) were used for 3D IF. Horseradish peroxidase (HRP)–conjugated secondary antibodies (Jackson ImmunoResearch, West Grove, PA) were used for Western blotting.

Transient transfection and Western blot

For LKB1 rescue experiments, H157 cells were transfected with either pCDNA3 empty GFP control vector or pEGFP-C1 LKB1 WT using Lipofectamine 2000 (Invitrogen), per manufacturer's protocol. For silencing experiments, H1299 or H1792 cells were transfected with either a scrambled control siRNA or siRNA targeting MARK1 (Sigma-Aldrich) or LKB1 (Sigma-Aldrich) using Oligofectamine (Invitrogen) or with siRNA targeting FAK (Sigma-Aldrich) using Lipofectamine 2000 (Invitrogen), per manufacturer's protocol. At 24 h later, cells were harvested and lysed with TNES buffer (50 mM Tris, pH 7.5, 100 mM NaCl, 2 mM EDTA, 1% NP-40) supplemented with Roche Complete Protease Inhibitor Cocktail (Roche, Indianapolis, IN) and a phosphatase inhibitor cocktail (10 mM sodium fluoride, 2 mM sodium pyrophosphate, 2 mM β-glycerophosphate, 200 nM sodium orthovanadate). Protein concentrations were determined using the bicinchoninic acid protein (BCA) assay kit (Pierce, Rockford, IL). A 30-µg amount of lysates was boiled in Laemmli sample buffer, loaded onto 10% SDS–PAGE gels, transferred onto polyvinyldifluoride (PVDF) membranes, blocked in 10% milk for 1 h at room temperature, and probed overnight at 4°C with primary antibodies diluted in either 5% bovine serum albumin (BSA) or nonfat dried milk, followed by appropriate HRP-conjugated secondary antibody and visualized using HyGlo Chemiluminescent HRP antibody detection (Denville, South Plainfield, NJ).

Generating 3D tumor spheroids

H1299 and H1792 cells with a stable or transient LKB1, MARK1, or FAK knockdown and corresponding controls, as well as H157 and HeLa cells stably expressing GFP-LKB1 or GFP-LKB1 plus constitutively active RhoA or cdc42, were grown to 70% confluency and then trypsinized, neutralized, and resuspended in complete RPMI (Invitrogen). To generate spheroids, 3000 cells in 200 µl (1.5×10^4 cells/ml) were added to a Spheron Nunclon 96-well plate (Thermo Scientific, Waltham, MA). At 3–4 d later, compacted spheroids were collected and resuspended in 2.0 mg/ml Collagen Type I (Advanced Biomatrix, San Diego, CA) and then plated in a Lab-Tek 8-well borosilicate bottom plate (Thermo Scientific) for immunofluorescence; a 35-mm glass-bottom dish (In Vitro Scientific, Sunnyvale, CA) for multiphoton microscopy; or a 6-well plate (Corning, Corning, NY) for Rho-GTPase activation assays. After the collagen solidified, complete RPMI was added to the top of the collagen matrix to provide a chemogradient for the spheroids.

Drug treatments

Spheroids formed from H1299 shLKB1 or pLKO.1 control cells were generated as described earlier. During embedding of spheroids in

the 3D collagen matrix, the FAK inhibitor PF-573228 (Sigma-Aldrich) was added at 1 μM or GM-6001 (Santa Cruz Biotechnology) was added at 20 μM to both the collagen and complete RPMI medium on top of the collagen matrix. DMSO was used as the vehicle control. Spheroids were incubated at 37°C and 5% CO_2 for 16–20 h to allow for invasion.

Rho-GTPase activation assays

Rho-GTPase activation assays were performed using H1299 and H157 cells, as previously described (Zhang *et al.*, 2008; Havel *et al.*, 2015). In brief, H1299 shLKB1 and pLKO.1 control spheroids were embedded in a 3D collagen matrix (2 mg/ml) as described earlier. At 0, 1, and 5 h postembedding, collagen was digested using collagenase (Sigma-Aldrich) at 37°C. Spheroids were centrifuged and supernatant discarded. Remaining cell pellets were lysed using Rho-GTPase activity assay lysis buffer supplemented with 100× protease inhibitor cocktail (Cytoskeleton). H1299 shLKB1 and pLKO.1, as well as H157 cells stably expressing empty GFP control or the various GFP-LKB1 constructs, as well as those coexpressing constitutively active RhoA or cdc42, were grown to 70% confluency. Cells were then trypsinized, and 2.0×10^6 cells were plated on a 10-cm fibronectin-coated plate (40 μg/ml). At 24 h later, cells were lysed using Rho-GTPase activity assay lysis buffer and 100× protease inhibitor (Cytoskeleton). In all cases, total protein quantification was determined using a BCA protein assay kit (Pierce). A 300-μg lysate was incubated with either GST-Rhotekin RBD beads (RhoA) or GST-PAK PBD beads (cdc42) for 1 h at 4°C. Pull-down and input samples (30 μg) were boiled in Laemmli sample buffer, loaded onto either 4–20% gradient (Bio-Rad, Hercules, CA) or 12% SDS–PAGE gels, transferred onto PVDF membranes, blocked in 5% milk for 1 h at room temperature, and probed overnight at 4°C with either mouse-RhoA (1:250 in Tris-buffered saline/Tween-20 [TBST]) or mouse-cdc42 (1:1000 in 0.1% milk) primary antibodies, followed by goat anti-mouse HRP-conjugated secondary antibody (1:10,000 in TBST) and visualized using HyGlo Chemiluminescent HRP antibody detection (Denville).

Three-dimensional spheroid immunofluorescence

Spheroids generated from either H1299 or H157 stable cells were embedded in a 3D collagen matrix as previously described. At 24 h later, cells were fixed using 4% paraformaldehyde (Electron Microscopy Sciences, Hatfield, PA) for 20 min at room temperature and then quenched with 0.1 M glycine in phosphate-buffered saline (PBS; Sigma-Aldrich) for 10 min. Spheroids were then permeabilized with 0.5% Triton-X (Promega, Madison, WI) for 1.5 h, washed with PBS for 10 min, and blocked with 5% normal goat serum (NGS; Jackson ImmunoResearch) for 1.5 h. H1299 and H157 spheroids were probed with rabbit $pFAK^{Y397}$ (1:200 in PBS with 1% BSA and 1% NGS) overnight at 4°C. Spheroids were then washed with PBS three times for 15 min each with vigorous shaking and probed with (H1299) Alexa Fluor 488 goat-anti-rabbit or (H157) Alexa Fluor 555 goat-anti-rabbit (1:750 in PBS with 1% NGS) for 1.5 h with gentle shaking at room temperature. H1299 spheroids were also probed with rabbit $pPaxillin^{Y118}$ (1:200 in PBS with 1% NGS) and Alexa Fluor 488 goat-anti-rabbit (1:750 in PBS with 1% NGS). After three PBS washes, all spheroids were then stained with 350 nM DAPI for 10 min, followed by three more PBS washes.

For 40× representative images for cell polarization, H157 and HeLa cells were first fixed with 4% paraformaldehyde and then quenched with 0.1 M glycine in PBS. Spheroids were then permeabilized with 0.5% Triton-X for 1.5 h, washed with PBS for 10 min, stained with Alexa Fluor 555–phalloidin (1:100 in PBS) overnight at 4°C, and then washed with PBS three times for 15 min each with vigorous shaking before imaging.

Microscopy

Wide-field imaging. For cell polarity experiments, still images of H1299, H1792, H157, and HeLa spheroids were acquired at 0 and 24 h using an Olympus IX51 at 4× (0.13 numerical aperture [NA] air), 10× (0.30 NA air), and 20× (0.45 NA air) using an Infinity2 charge-coupled device (CCD) camera (Lumenera, Ottawa, Canada).

Confocal imaging. To quantify cell meandering and velocity, H1299 spheroids and H157 spheroids reexpressing GFP-LKB1 NTD, NTD-kinase, kinase domain, and kinase-CTD were imaged using a PerkinElmer (Waltham, MA) Ultraview spinning-disk confocal microscope at 10× (Plan-Neofluar, 0.30 NA) mounted onto a Zeiss (Jena, Germany) Axiovert encased at 37°C with 5% CO_2. Transmitted light images were acquired every 10 min for 20 h with 10-μm *z*-stack intervals using a Hamamatsu (Hamamatsu, Japan) Orca ER CCD camera with 2×2 binning. H157 spheroids reexpressing empty GFP control, GFP-LKB1 wild type, C430S, K78I, K78I-C430S, CTD, and CTD-C430S were imaged using a Leica (Wetzlar, Germany) TCS SP8 inverted confocal microscope with live-cell chamber at 10× (HC Plan Fluotar, 0.30 NA), acquiring images every 10 min for 24 h with 5-μm *z*-stack intervals using a 488-nm argon laser under resonance scanning (8 kHz, 32 averaging). Representative images for H157 cell polarization were acquired using a Leica SP8 inverted confocal microscope at 40× (HP PL APO, 1.30 NA oil) using a 514-nm argon laser.

For 3D immunofluorescence imaging, H1299 spheroids were imaged using the FV1000 inverted confocal mounted on an Olympus (Tokyo, Japan) IX81 inverted microscope (40×, 0.90 NA, Water PlanApo) with 1.3-μm *z*-stack intervals and sequential scanning (405, 488 nm). H157 spheroids were imaged with the Leica TCS SP8 inverted confocal microscope (40× oil HC PL APO, 1.30 NA) using 1.3-μm *z*-stack intervals and sequential scanning (405-nm DMOD Flexible, 488-nm argon, 514-nm argon) at 600 Hz with 4 averaging.

Multiphoton imaging. Spheroids of H1299 shLKB1 and pLKO.1 or H157 stable cells were dyed using 1 μM Red CellTracker (Invitrogen). The H1299 stable spheroids were imaged at 0, 6, and 24 h postinvasion, and H157 stable spheroids were imaged at 0 and 24 h postinvasion, using a standard upright Zeiss Axio Examiner Z1 microscope with 20× water immersion objective (1.0 NA DIC (UV) VIS-IR). The second harmonic generation (SHG) signal was obtained using a bandpass 380- to 430-nm cube. To image the cells stained with Red CellTracker, a bandpass of 570- to 610-nm cube with a long pass of 550 nm was used. Images were taken with a Coherent (Santa Clara, CA) Chameleon Verdi laser at 790-nm wavelength. *z*-stack images were taken with a 1-μm interval.

Image analysis

Cell polarity was calculated using ImageJ/Fiji (National Institutes of Health, Bethesda, MD), where an invading cell was considered to have a mesenchymal polarity if its length was greater than or equal to twice its width (Nogawa and Mizuno, 1981; Ladhani *et al.*, 2011). Polarity of H1299 shLKB1 was compared with that of pLKO.1 control, as was polarity of H1299 stable cells in response to FAK inhibition, using the two-tailed Student's *t* test with a *p* value of 0.05. Each H157 and HeLa GFP-LKB1 cell line was compared with the respective empty GFP control lines and also to its farnesylation mutant partner

(WT vs. C430S, K78I vs. K78I-C430S, CTD vs. CTD-C430S) using Fisher's exact test with a p value of 0.05. *$p \leq 0.05$, **$p \leq 0.01$, ***$p \leq 0.001$, and ****$p \leq 0.0001$,

For H1299 cells, Volocity (PerkinElmer) image analysis software and manual tracking was used to quantify total invasion (FAK inhibitor experiment), cell velocity, and meandering index (displacement/distance) as a means of determining directional persistence. The total number of cells invaded in response to FAK inhibition was compared between H1299 shLKB1 and pLKO.1 control, as was the difference in velocity of mesenchymal and amoeboid cells from H1299 shLKB1 and pLKO.1 control cells upon FAK inhibition. For H157 cells, 30 cells for each condition were tracked using automated tracking through the Spots function with Brownian motion, with a maximum distance of 20 µm and a gap size of 2. Cell velocity and meandering of H1299 shLKB1 were compared with those for pLKO.1 control using the two-tailed Student's t test with a p value of 0.05. Each H157 GFP-LKB1 cell line was compared with both the H157 empty GFP control line and its respective farnesylation mutant (as described earlier), whereas cell lines coexpressing constitutively active RhoA or cdc42 were compared with their isogenic partner line and empty GFP control cells using the two-tailed Student's t test with a p value of 0.05. *$p \leq 0.05$, **$p \leq 0.01$, and ****$p \leq 0.0001$.

Phospho-FAK and phospho-paxillin levels were analyzed with the vesicle-tracking feature in Imaris Cell (Bitplane, South Windsor, CT). Phospho-FAK sites in H1299 pLKO.1 and shLKB1 cells were quantified with quality ranging from 438 to 1201 (16-bit imaging) and minimum region threshold of 25. In H1299 MARK1 siRNA and siRNA control cells, pFAK sites were quantified with quality ranging from 297 to 1073 (16-bit imaging) and minimum region threshold of 14.5. H157-cell pFAK sites were thresholded with quality ranging from 54.3 to 255 (8-bit imaging) and minimum region threshold of 70.12. pPaxillin sites in H1299 pLKO.1 and shLKB1 cells were quantified with thresholding ranging from 333 to 1335 (16-bit imaging) and minimum region threshold of 33.1. Mean pFAK and pPaxillin intensity and number of sites per cell of H1299 shLKB1 were compared with those for pLKO.1 control, and each H157 GFP-LKB1 cell line was compared with H157 empty GFP control cells using the two-tailed Student's t test with a p value of 0.05. *$p \leq 0.05$ and ****$p \leq 0.0001$.

Quantification of collagen alignment

A novel local alignment coefficient was used to quantify the heterogeneous alignment patterns. The collagen fibers in microscopy images were extracted using the CT-FIRE software (Bredfeldt *et al.*, 2014). All fibers were quantized with a 5-pixel length. The local alignment coefficient was measured for every pixel in the x- and y-axes of all z-stack images. (Supplemental Figure S7 explains the definition of the local alignment coefficient and the choice of optimal measurement parameters.) A local alignment value of 0 means that the fiber angular distribution is isotropic with no bias in any orientation or the number of fibers in a local circular bin is below a threshold and considered too few to count. A local alignment value of 1 means that all the fibers are perfectly aligned. Histograms of local alignment coefficients, surface plots, and contour plots were generated. When comparing between different time points, we normalized to the 0-h measurements and plotted the difference in histograms to show the changes in the alignment distribution.

ACKNOWLEDGMENTS

We thank Stefan Kaluz for assistance with cloning, the Emory Integrated Cellular Imaging Core for assistance with microscopy, and the Emory Custom Cloning Core Facility for providing GFP-tagged plasmids. J.K. is supported by the National Institutes of Health under Ruth L. Kirschstein National Research Service Award 1F31CA180511. S.W. is supported by the National Institutes of Health under Ruth L. Kirschstein National Research Service Award 1F31CA200383-01. S.W. was previously supported by a National Science Foundation Graduate Research Fellowship under Grant DGE-0940903. S.W. and J.K. are partially supported by Laney Graduate School. B.L. and Y.J. are supported partially by National Institutes of Health/National Cancer Institute Grant 1U01CA143069. W.Z. is supported by the National Cancer Institute (R01CA140571). This work was supported by National Cancer Institute awards (1R01CA1428580, 1R01CA201340, 1R01CA194027) to A.I.M. Research reported in this article was supported in part by the Winship Cancer Institute and Emory Integrated Cellular Imaging Core and the National Institutes of Health/National Cancer Institute under Award P30CA138292.

REFERENCES

Amin N, Khan A, St Johnston D, Tomlinson I, Martin S, Brenman J, McNeill H (2009). LKB1 regulates polarity remodeling and adherens junction formation in the Drosophila eye. Proc Natl Acad Sci USA 106, 8941–8946.

Asada N, Sanada K, Fukada Y (2007). LKB1 regulates neuronal migration and neuronal differentiation in the developing neocortex through centrosomal positioning. J Neurosci 27, 11769–11775.

Baas AF, Kuipers J, van der Wel NN, Batlle E, Koerten HK, Peters PJ, Clevers HC (2004). Complete polarization of single intestinal epithelial cells upon activation of LKB1 by STRAD. Cell 116, 457–466.

Barnes AP, Lilley BN, Pan YA, Plummer LJ, Powell AW, Raines AN, Sanes JR, Polleux F (2007). LKB1 and SAD kinases define a pathway required for the polarization of cortical neurons. Cell 129, 549–563.

Brajenovic M, Joberty G, Kuster B, Bouwmeester T, Drewes G (2004). Comprehensive proteomic analysis of human Par protein complexes reveals an interconnected protein network. J Biol Chem 279, 12804–12811.

Bredfeldt JS, Liu Y, Conklin MW, Keely PJ, Mackie TR, Eliceiri KW (2014). Automated quantification of aligned collagen for human breast carcinoma prognosis. J Pathol Inform 5, 28.

Cancer Genome Atlas Research Network (2014). Comprehensive molecular profiling of lung adenocarcinoma. Nature 511, 543–550.

Carretero J, Shimamura T, Rikova K, Jackson AL, Wilkerson MD, Borgman CL, Buttarazzi MS, Sanofsky BA, McNamara KL, Brandstetter KA, *et al.* (2010). Integrative genomic and proteomic analyses identify targets for Lkb1-deficient metastatic lung tumors. Cancer Cell 17, 547–559.

Chan KT, Asokan SB, King SJ, Bo T, Dubose ES, Liu W, Berginski ME, Simon JM, Davis IJ, Gomez SM, *et al.* (2014). LKB1 loss in melanoma disrupts directional migration toward extracellular matrix cues. J Cell Biol 207, 299–315.

Cheng H, Liu P, Wang ZC, Zou L, Santiago S, Garbitt V, Gjoerup OV, Iglehart JD, Miron A, Richardson AL, *et al.* (2009). SIK1 couples LKB1 to p53-dependent anoikis and suppresses metastasis. Sci Signal 2, ra35–ra35.

Ding L, Getz G, Wheeler DA, Mardis ER, McLellan MD, Cibulskis K, Sougnez C, Greulich H, Muzny DM, Morgan MB, *et al.* (2008). Somatic mutations affect key pathways in lung adenocarcinoma. Nature 455, 1069–1075.

Erler JT, Bennewith KL, Nicolau M, Dornhofer N, Kong C, Le Q-T, Chi J-TA, Jeffrey SS, Giaccia AJ (2006). Lysyl oxidase is essential for hypoxia-induced metastasis. Nature 440, 1222–1226.

Etienne-Manneville S (2004). Cdc42—the centre of polarity. J Cell Sci 117, 1291–1300.

Friedl P, Wolf K (2003). Tumour-cell invasion and migration: diversity and escape mechanisms. Nat Rev Cancer 3, 362–374.

Friedl P, Zanker KS, Brocker EB (1998). Cell migration strategies in 3-D extracellular matrix: differences in morphology, cell matrix interactions, and integrin function. Microsc Res Tech 43, 369–378.

Gadea G, de Toledo M, Anguille C, Roux P (2007). Loss of p53 promotes RhoA–ROCK-dependent cell migration and invasion in 3D matrices. J Cell Biol 178, 23–30.

Gao Y, Xiao Q, Ma H, Li L, Liu J, Feng Y, Fang Z, Wu J, Han X, Zhang J, *et al.* (2010). LKB1 inhibits lung cancer progression through lysyl oxidase and extracellular matrix remodeling. Proc Natl Acad Sci USA 107, 18892–18897.

Goodwin JM, Svensson RU, Lou HJ, Winslow MM, Turk BE, Shaw RJ (2014). An AMPK-independent signaling pathway downstream of the LKB1 tumor suppressor controls snail1 and metastatic potential. Mol Cell 55, 436–450.
Guldberg P, thor Straten P, Ahrenkiel V, Seremet T, Kirkin AF, Zeuthen J (1999). Somatic mutation of the Peutz-Jeghers syndrome gene, LKB1/STK11, in malignant melanoma. Oncogene 18, 1777–1780.
Han X, Li F, Fang Z, Gao Y, Li F, Fang R, Yao S, Sun Y, Li L, Zhang W, *et al.* (2014). Transdifferentiation of lung adenocarcinoma in mice with Lkb1 deficiency to squamous cell carcinoma. Nat Commun 5, 3261.
Hardie DG, Alessi DR (2013). LKB1 and AMPK and the cancer-metabolism link—ten years after. BMC Biol 11, 36.
Haston WS, Shields JM, Wilkinson PC (1982). Lymphocyte locomotion and attachment on two-dimensional surfaces and in three-dimensional matrices. J Cell Biol 92, 747–752.
Havel LS, Kline ER, Salgueiro AM, Marcus AI (2015). Vimentin regulates lung cancer cell adhesion through a VAV2-Rac1 pathway to control focal adhesion kinase activity. Oncogene 34, 1979–1390.
Hawley SA, Boudeau J, Reid JL, Mustard KJ, Udd L, Makela TP, Alessi DR, Hardie DG (2003). Complexes between the LKB1 tumor suppressor, STRAD alpha/beta and MO25 alpha/beta are upstream kinases in the AMP-activated protein kinase cascade. J Biol 2, 28.
Hezel AF, Bardeesy N (2008). LKB1; linking cell structure and tumor suppression. Oncogene 27, 6908–6919.
Houde VP, Ritorto MS, Gourlay R, Varghese J, Davies P, Shpiro N, Sakamoto K, Alessi DR (2014). Investigation of LKB1 Ser431 phosphorylation and Cys433 farnesylation using mouse knockin analysis reveals an unexpected role of prenylation in regulating AMPK activity. Biochem J 458, 41–56.
Huang YW, Baluna R, Vitetta ES (1997). Adhesion molecules as targets for cancer therapy. Histol Histopathol 12, 467–477.
Jaleel M, McBride A, Lizcano JM, Deak M, Toth R, Morrice NA, Alessi DR (2005). Identification of the sucrose non-fermenting related kinase SNRK, as a novel LKB1 substrate. FEBS Lett 579, 1417–1423.
Ji H, Ramsey MR, Hayes DN, Fan C, McNamara K, Kozlowski P, Torrice C, Wu MC, Shimamura T, Perera SA, *et al.* (2007). LKB1 modulates lung cancer differentiation and metastasis. Nature 448, 807–810.
Kakiuchi M, Nishizawa T, Ueda H, Gotoh K, Tanaka A, Hayashi A, Yamamoto S, Tatsuno K, Katoh H, Watanabe Y, *et al.* (2014). Recurrent gain-of-function mutations of RHOA in diffuse-type gastric carcinoma. Nat Genet 46, 583–587.
Kishi M, Pan YA, Crump JG, Sanes JR (2005). Mammalian SAD kinases are required for neuronal polarization. Science 307, 929–932.
Kline ER, Shupe J, Gilbert-Ross M, Zhou W, Marcus AI (2013). LKB1 represses focal adhesion kinase (FAK) signaling via a FAK-LKB1 complex to regulate FAK site maturation and directional persistence. J Biol Chem 288, 17663–17674.
Kosla J, Pankova D, Plachy J, Tolde O, Bicanova K, Dvorak M, Rosel D, Brabek J (2013). Metastasis of aggressive amoeboid sarcoma cells is dependent on Rho/ROCK/MLC signaling. Cell Commun Signal 11, 51.
Ladhani O, Sanchez-Martinez C, Orgaz JL, Jimenez B, Volpert OV (2011). Pigment epithelium-derived factor blocks tumor extravasation by suppressing amoeboid morphology and mesenchymal proteolysis. Neoplasia 13, 633–642.
Li J, Liu J, Li P, Mao X, Li W, Yang J, Liu P (2014). Loss of LKB1 disrupts breast epithelial cell polarity and promotes breast cancer metastasis and invasion. J Exp Clin Cancer Res 33, 70.
Lizcano JM, Goransson O, Toth R, Deak M, Morrice NA, Boudeau J, Hawley SA, Udd L, Makela TP, Hardie DG, *et al.* (2004). LKB1 is a master kinase that activates 13 kinases of the AMPK subfamily, including MARK/PAR-1. EMBO J 23, 833–843.
Lo B, Strasser G, Sagolla M, Austin CD, Junttila M, Mellman I (2012). Lkb1 regulates organogenesis and early oncogenesis along AMPK-dependent and -independent pathways. J Cell Biol 199, 1117–1130.
Mandeville JT, Lawson MA, Maxfield FR (1997). Dynamic imaging of neutrophil migration in three dimensions: mechanical interactions between cells and matrix. J Leukoc Biol 61, 188–200.
Marcus AI, Zhou W (2010). LKB1 regulated pathways in lung cancer invasion and metastasis. J Thorac Oncol 5, 1883–1886.
Martin SG, St Johnston D (2003). A role for Drosophila LKB1 in anterior-posterior axis formation and epithelial polarity. Nature 421, 379–384.
Matsumoto S, Iwakawa R, Takahashi K, Kohno T, Nakanishi Y, Matsuno Y, Suzuki K, Nakamoto M, Shimizu E, Minna JD, *et al.* (2007). Prevalence and specificity of LKB1 genetic alterations in lung cancers. Oncogene 26, 5911–5918.
Morley S, Hager MH, Pollan SG, Knudsen B, Di Vizio D, Freeman MR (2014). Trading in your spindles for blebs: the amoeboid tumor cell phenotype in prostate cancer. Asian J Androl 16, 530–535.
Nakano A, Takashima S (2012). LKB1 and AMP-activated protein kinase: regulators of cell polarity. Genes Cells 17, 737–747.
Nogawa H, Mizuno T (1981). Mesenchymal control over elongating and branching morphogenesis in salivary gland development. J Embryol Exp Morphol 66, 209–221.
Parri M, Chiarugi P (2010). Rac and Rho GTPases in cancer cell motility control. Cell Commun Signal 8, 23.
Partanen JI, Tervonen TA, Myllynen M, Lind E, Imai M, Katajisto P, Dijkgraaf GJ, Kovanen PE, Makela TP, Werb Z, *et al.* (2012). Tumor suppressor function of Liver kinase B1 (Lkb1) is linked to regulation of epithelial integrity. Proc Natl Acad Sci USA 109, E388–E397.
Rosel D, Brabek J, Tolde O, Mierke CT, Zitterbart DP, Raupach C, Bicanova K, Kollmannsberger P, Pankova D, Vesely P, *et al.* (2008). Up-regulation of Rho/ROCK signaling in sarcoma cells drives invasion and increased generation of protrusive forces. Mol Cancer Res 6, 1410–1420.
Roy BC, Kohno T, Iwakawa R, Moriguchi T, Kiyono T, Morishita K, Sanchez-Cespedes M, Akiyama T, Yokota J (2010). Involvement of LKB1 in epithelial-mesenchymal transition (EMT) of human lung cancer cells. Lung Cancer 70, 136–145.
Sahai E, Marshall CJ (2003). Differing modes of tumour cell invasion have distinct requirements for Rho/ROCK signalling and extracellular proteolysis. Nat Cell Biol 5, 711–719.
Sanchez-Cespedes M, Parrella P, Esteller M, Nomoto S, Trink B, Engles JM, Westra WH, Herman JG, Sidransky D (2002). Inactivation of LKB1/STK11 is a common event in adenocarcinomas of the lung. Cancer Res 62, 3659–3662.
Shaw RJ, Kosmatka M, Bardeesy N, Hurley RL, Witters LA, DePinho RA, Cantley LC (2004). The tumor suppressor LKB1 kinase directly activates AMP-activated kinase and regulates apoptosis in response to energy stress. Proc Natl Acad Sci USA 101, 3329–3335.
Spicer J, Rayter S, Young N, Elliott R, Ashworth A, Smith D (2003). Regulation of the Wnt signalling component PAR1A by the Peutz-Jeghers syndrome kinase LKB1. Oncogene 22, 4752–4756.
Vallenius T, Vaahtomeri K, Kovac B, Osiceanu A-M, Viljanen M, Mäkelä TP (2011). An association between NUAK2 and MRIP reveals a novel mechanism for regulation of actin stress fibers. J Cell Sci Suppl 124, 384–393.
Wang K, Yuen ST, Xu J, Lee SP, Yan HHN, Shi ST, Siu HC, Deng S, Chu KM, Law S, *et al.* (2014). Whole-genome sequencing and comprehensive molecular profiling identify new driver mutations in gastric cancer. Nat Genet 46, 573–582.
Watts JL, Morton DG, Bestman J, Kemphues KJ (2000). The C. elegans par-4 gene encodes a putative serine-threonine kinase required for establishing embryonic asymmetry. Development 127, 1467–1475.
Wingo SN, Gallardo TD, Akbay EA, Liang MC, Contreras CM, Boren T, Shimamura T, Miller DS, Sharpless NE, Bardeesy N, *et al.* (2009). Somatic LKB1 mutations promote cervical cancer progression. PLoS One 4, e5137.
Wolf K, Mazo I, Leung H, Engelke K, von Andrian UH, Deryugina EI, Strongin AY, Bröcker E-B, Friedl P (2003a). Compensation mechanism in tumor cell migration: mesenchymal–amoeboid transition after blocking of pericellular proteolysis. J Cell Biol 160, 267–277.
Wolf K, Müller R, Borgmann S, Bröcker E-B, Friedl P (2003b). Amoeboid shape change and contact guidance: T-lymphocyte crawling through fibrillar collagen is independent of matrix remodeling by MMPs and other proteases. Blood 102, 3262–3269.
Wyckoff JB, Pinner SE, Gschmeissner S, Condeelis JS, Sahai E (2006). ROCK- and myosin-dependent matrix deformation enables protease-independent tumor-cell invasion in vivo. Curr Biol 16, 1515–1523.
Xu X, Jin D, Durgan J, Hall A (2013). LKB1 controls human bronchial epithelial morphogenesis through p114RhoGEF dependent RhoA activation. Mol Cell Biol 33, 2671–2682.
Xu X, Omelchenko T, Hall A (2010). LKB1 tumor suppressor protein regulates actin filament assembly through Rho and its exchange factor Dbl independently of kinase activity. BMC Cell Biol 11, 77.
Yoon KA, Ku JL, Choi HS, Heo SC, Jeong SY, Park YJ, Kim NK, Kim JC, Jung PM, Park JG (2000). Germline mutations of the STK11 gene in Korean Peutz-Jeghers syndrome patients. Br J Cancer 82, 1403–1406.
Zagórska A, Deak M, Campbell DG, Banerjee S, Hirano M, Aizawa S, Prescott AR, Alessi DR (2010). New roles for the LKB1-NUAK pathway in controlling myosin phosphatase complexes and cell adhesion. Sci Signal 3, ra25.
Zhang S, Schafer-Hales K, Khuri FR, Zhou W, Vertino PM, Marcus AI (2008). The tumor suppressor LKB1 regulates lung cancer cell polarity by mediating cdc42 recruitment and activity. Cancer Res 68, 740–748.